Version of Wednesday 3rd May, 2023, 14:49

TECHNIQUES FOR CONTINUOUS OPTIMAL TRANSPORT PROBLEM

LUCA DIECI AND DANIYAR OMAROV

Abstract. In this work, we consider and compare several different numerical methods to solve the classic continuous optimal transport problem between two probability densities, while minimizing the cost function given by the squared Euclidean distance. Classically, the problem reduces to having to solve a second order elliptic PDE (the Monge-Ampére PDE). An alternative is to consider the so-called fluid dynamics formulation of Benamou and Brenier. One of our goals in this work is to compare two numerical methods used for the fluid-dynamics formulation with a direct discretization of the Monge-Ampére PDE. Finally, we introduce a very natural new class of problems, which we call *separable*, for which we devise very accurate methods. We give implementation details of all the different methods, and extensive testing on many different problems which we created in order to provide a fairly complete arrays of the typical difficulties one encounters, and to highlight the benefits of different methods. With the same level of attention to implementation details, some insight into the relative merits of the different techniques emerges and we can draw conclusions and provide recommendations on what techniques to adopt for this problem.

1. Introduction

Optimal transport (OT) problems appear in several applications in various fields, such as machine learning, mathematical biology, economics, and image processing (e.g., see [18], [21], and the references in [23]). Indeed, the pervasive nature of OT problems has led to a lot of interest in numerical OT, and new methods continue to be developed for this task (see the many references below). However, all the numerical works of which we are aware seem to be concerned with novel algorithmic developments but not with providing a comparison of these new developments with alternative, pre-existing techniques. This gap has provided the motivation for our work, and as far as we know our is a first effort to compare methods for the OT problems.

The first mass transfer problem, a civil engineering problem, was considered by Monge in 1781, [20]. A modern treatment of this problem, in term of probability densities, was formulates by Kantorovich in [11], who opened the path to viewing the problem in the framework of an optimization task and to exploit duality, which allowed for great improvements in the theory, and also to obtain powerful numerical methods.

A useful formulation of the problem considers two given probability densities, $\rho_0(x)$, $x \in \Omega$, and $\rho_1(y)$, $y \in \Omega$, where Ω is a convex and compact subset of $\mathbb{R}^d$. Then, the optimal transport problem consists in seeking an invertible map $T : \Omega \to \Omega$ which transports one density into the other[1], while minimizing a given cost functional $c(x, y)$ which represents the cost of moving one unit of mass x into one unit y. In this work, we will only consider the case of dimensions $d = 1$ or $d = 2$, and continuous

1991 *Mathematics Subject Classification.* 65N99, 49N99.

Key words and phrases. Continuous optimal transport, numerical methods, Monge–Ampére, fluid flow, separable, Wasserstein distance, squared Euclidean cost.

The authors are grateful to Jianbo Cui for sharing his code and for helpful comments during the preparation of this manuscript.

[1]By this, it is meant that T pushes ρ_0 forward to ρ_1, that is $\rho_0(T^{-1}(A)) = \rho_1(A)$ for all Borel sets $A \subset \Omega$

densities ρ_0 and ρ_1, though –in general– also the case of ρ_0 and ρ_1 being discrete densities is of interest. Finally, although the cost may be just Euclidean distance or any other p-norm with $p > 1$, for us in this work the cost is given by the squared Euclidean distance, that is $c(x, y) = \|x - y\|_2^2$. This is the most widely studied OT problem, and it is well known that this problem has a unique solution; that is, there is a unique smooth, invertible, map T minimizing the cost, see references below. We will henceforth just restrict to this case, and so we will just write $\|\cdot\|^2$ rather than $\|\cdot\|_2^2$.

To recap, the Monge-Kantorovich (or just MK) problem we consider consists of the following.

1. Given $\rho_0(x) \geq 0$, $\rho_1(x) \geq 0$, such that $\int_\Omega \rho_0(x)dx = \int_\Omega \rho_1(x)dx = 1$, where $\Omega \subset \mathbb{R}^d$ is compact and convex.
2. Seek a smooth, invertible, map $T : \Omega \to \Omega$ which achieves

$$\begin{aligned} &\inf_{T:\Omega\to\Omega} \int_\Omega \|x - T(x)\|^2 \rho_0(x)dx \\ &\text{s. t.} \int_{x\in A} \rho_1(x)dx = \int_{T^{-1}(x)\in A} \rho_0(x)dx \ , \text{ for every bounded set } A \subset \Omega, \end{aligned} \tag{1}$$

so that, from the change of variable formula. the last relation rewrites as

$$\rho_1(T(x)) \det(\nabla T(x)) = \rho_0(x) \ .$$

In the specific case we are considering here, the unique optimal map T is the gradient of a convex function u (see [23, Theorem 1.17]). In light of this, the change of variable formula rewrites as the following nonlinear elliptic partial differential equation (PDE), the *Monge-Ampére* equation (MA for short):

$$\begin{aligned} &\det(D^2u(x))\rho_1(\nabla u(x)) = \rho_0(x) \\ &\text{where } u(x) \text{ is convex and } D^2u \text{ is its Hessian.} \end{aligned} \tag{2}$$

We will shortly discuss appropriate boundary conditions (BCs) for this PDE, at which point a possible method will suggest itself.

An alternative formulation of the OT problem was given by Benamou & Brenier in [1], where they showed that the OT problem is equivalent to the following constrained variational problem (see [23, Theorem 5.28]):

$$\begin{aligned} &\inf_v \int_0^1 \int_\Omega \|v(t,x)\|^2 \rho(t,x)dxdt \quad \text{such that} \\ &\frac{\partial \rho(t,x)}{\partial t} + \nabla \cdot (v(t,x)\rho(t,x)) = 0 \quad \text{and} \\ &\rho(0,x) = \rho_0(x), \quad \rho(1,x) = \rho_1(x) \end{aligned} \tag{3}$$

where $v(t, x)$ is a smooth velocity field, and $\rho(t, x)$ is a density interpolation function. The minimization problem (3) is known as Benamou-Brenier formulation or fluid dynamics formulation. The relation between the minimization problem (3) and the result giving the optimal map T as gradient of a convex function u is that $\nabla u(x) = x + v(0, x)$ (again, see cited references). The optimal value of the functional in (3) is the square of the (L^2-)Wasserstein distance between ρ_0 and ρ_1, and it is usually written as $g_W^2(\rho_0, \rho_1)$. This distance g_W has become a popular way to measure distance between distributions, thanks to its increasing use in statistics and machine learning, e.g., in generative adversarial networks (GAN).

Remark 1.1. $[\Omega = \mathbb{R}^d]$ *An important case is when the problem is set on the full space* $\mathbb{R}^d$*, that is* $\Omega = \mathbb{R}^d$ *in the above. Now we will need to require that* ρ_0 *and* ρ_1 *have finite second moments:* $\int_{\mathbb{R}^d} \|x\|^2 \rho_0(x)dx$, $\int_{\mathbb{R}^d} \|x\|^2 \rho_1(x)dx < \infty$*. With this, the existence (and uniqueness) of the optimal map* $T : \mathbb{R}^d \to \mathbb{R}^d$ *continues to hold; see [23, Theorem 1.22]. Likewise, the previous equivalence result, that is* $\nabla u(x) = x + v(0; x)$*, about the formulations* (2) *and* (3) *holds as well.*

Remark 1.2. *Although we are only considering the continuous optimal transport problem, depending on whether (one or both of) the densities are discrete or continuous, one has a fully discrete, or a semi-discrete, or a continuous problem. Naturally, different methods apply in these different situations. For example, when mapping a discrete density to a discrete density, the resulting discrete OT problem reduces to an assignment (linear programming) problem and we refer to [3] and [7] for viable techniques. When mapping a continuous density to a discrete density, one has a so-called semi-discrete OT problem, which boils down to finding a Laguerre tessellation, and we refer to [8], as well as [17] and [13] for a review of numerical techniques in this case. Although there are efficient techniques in the discrete and semi-discrete cases, for a truly continuous optimal transport problem (that is, when both* ρ_0 *and* ρ_1 *are) we see at least two major difficulties in transitioning from the continuous transport problem to a fully (or semi) discrete problem: (1) where and how to sample the continuous densities, and (2) how to extract the optimal map from the joint distribution obtained solving the discrete problem. As far as we can tell, these two tasks are not generally settled, and that is why we stuck with techniques designed for the continuous OT problem.*

The rest of this paper is organized as follows: in Section 2, we first discuss at a high level (Section 2.1) the three basic numerical methods which we considered for solving the OT problem and then (in Section 2.2), we give details of their numerical implementation. In Section 3, we introduce a simple but important class of problems for which one can always solve 1-d (and not 2-d) problems and the numerical methods considered (especially one of them) become particularly efficient; we also give details on the well-posedness of these 1-d problems in an Appendix at the end. In Section 4, we give a list of problems we created as well as numerical results. Conclusions are in Section 5.

2. Algorithms

Below, we review three basic techniques to solve the OT problem based on either solving the Monge-Ampere PDE, or using the Benamou-Brenier formulation, or using a system of PDEs also resulting from the Benamou-Brenier formulation.

2.1. **Basic Algorithms Description.**

2.1.1. *Monge-Ampere PDE.* The most direct approach to find the Monge map is to solve (a discretized version of) (2). This has been done many times before; e.g., see [4, 22] for early work, [16] as well as [5, 9, 10, 19] for more recent discretization efforts, as well as the reformulation as a steady-state of an associated parabolic problem of [24]. In this work, we will closely follow the algorithm proposed by Froese in [9]. Before discussing more details, including the choice of BCs, we note that there are two other issues of concern. First of all, since uniqueness is guaranteed only for the map $T(x)$, a solution $u(x)$ of (2) is unique only up to a constant. In practice, one can remove this non-uniqueness in several ways: for example, by enforcing that the solution has mean zero ($\int_\Omega u(x)dx = 0$) or by fixing a specific

value a-priori (say, $u(x_0) = 0$). In [9], the mean zero condition was implemented. The second concern is that we are interested in a convex solution u. A main contribution of [9] on this aspect is related to the discretization of the determinant operator. In fact, a straightforward discretization of (2) by centered differences methods will not conserve convexity of the solution during iterations. Froese in [9] resolves this issue by replacing the determinant operator with the following, and then using centered difference (see Section 2.2.1)

$$\det^+(D^2u(x)) = \min_{(v_1,v_2)\in V} \Big\{ \max(u_{v_1v_1}, 0) \max(u_{v_2v_2}, 0) + \min(u_{v_2v_2}, 0) + \min(u_{v_2v_2}, 0) \Big\} \tag{4}$$

where V is the set of all orthonormal bases of $\mathbb{R}^2$. Under this specific discretization, Froese gives some convergence results for the finite difference scheme (see [9, Theorem 5]).

2.1.2. *Regularized Benamou-Brenier.* The next algorithm we considered is based upon the optimization problem expressed by (3). The basic approach based on solving this optimization problem was discussed already in the original paper [1] where the authors confronted the difficulties arising from lack of strict convexity of the functional. In our presentation, we will follow the recent work of Li et al., [14], where the authors expand upon the work [1].

To begin with, the authors of [14] replace (as already done in [1]) the velocity field function v with the flux function m:

$$v(t,x) = \frac{m(t,x)}{\rho(t,x)}$$

and (3) can be reformulates as

$$\begin{aligned} &\min_{m,\rho} \int_0^1 \int_\Omega \left|\left| \frac{m(t,x)}{\rho(t,x)} \right|\right|_2^2 \rho(t,x) dx dt \\ &\frac{\partial \rho(t,x)}{\partial t} + \nabla \cdot m(t,x) = 0 \\ &\rho(0,x) = \rho_0(x), \quad \rho(1,x) = \rho_1(x), \end{aligned} \tag{5}$$

where the infimum is sought among the flux functions m satisfying zero-flux conditions, [14]. Next, motivated by the lack of strict convexity and by the fact that if $\rho(t,x)$ becomes 0 (or even close to 0), a numerical scheme will run into difficulties, the authors in [14] regularize (5) as follows. They perform the change of variable $m(t,x) = \widetilde{m}(t,x) + \beta \nabla \rho(t,x)$, where β is a regularization parameter, and rewrite (5) as:

$$\begin{aligned} &\min_{\widetilde{m},\rho} \int_0^1 \int_\Omega \Big\{ \frac{||\widetilde{m}(t,x)||^2}{\rho(t,x)} + \beta^2 (\nabla \log \rho(t,x))^2 \rho(t,x) \Big\} dx dt + 2\beta \mathcal{D}(\rho_1|\rho_0) \\ &\frac{\partial \rho(t,x)}{\partial t} + \nabla \cdot \widetilde{m}(t,x) = 0 \\ &\rho(0,x) = \rho_0(x), \quad \rho(1,x) = \rho_1(x), \end{aligned} \tag{6}$$

where $\mathcal{D}(\rho_1|\rho_0)$ is the constant

$$\mathcal{D}(\rho_1|\rho_0) = \int_\Omega \rho_1(x) \log \rho_1(x) dx - \int_\Omega \rho_0(x) \log \rho_0(x) dx.$$

We note that with this reformulation the Wasserstein distance $g_W(\rho_0, \rho_1)$ is thus approximated by the square root of the minimum value in (6).

The chief difference between (5) and (6) is the *Fisher information* term $\mathcal{I}(\rho)$:

$$\mathcal{I}(\rho) = \int_0^1 \int_\Omega (\nabla \log \rho(t,x))^2 \rho(t,x) dx dt \ .$$

The purpose of this regularization is that adding the Fisher information term maintains the probability densities strictly positive (it acts as a barrier function), and further introduces strict convexity into the original minimization problem. Some convergence results as $\beta \to 0$ of the solution of (6) to that of (5) are in [12]. But, of course, in practice one cannot let $\beta \to 0$ and balancing the appropriate value of β with the discretization level in x and t will be important; see Table 1, which clearly shows the need to decrease β up to the discretization error level in space and time, but that there is no benefit beyond that.

	dt = 1/6			**dt = 1/11**			**dt = 1/21**		
$\boldsymbol{\beta}$	**dx = 1/16**	**dx = 1/32**	**dx = 1/64**	**dx = 1/16**	**dx = 1/32**	**dx = 1/64**	**dx = 1/16**	**dx = 1/32**	**dx = 1/64**
$\mathbf{10^{-1}}$	0.550	0.563	0.567	0.553	0.564	0.567	0.555	0.566	0.569
$\mathbf{10^{-2}}$	0.053	0.046	0.050	0.054	0.052	0.056	0.056	0.054	0.058
$\mathbf{10^{-4}}$	0.028	0.020	0.017	0.031	0.017	0.010	0.036	0.021	0.011
$\mathbf{10^{-8}}$	0.028	0.021	0.018	0.031	0.017	0.010	0.036	0.021	0.011

TABLE 1. Errors in Optimal Map for Problem 4.1, obtained by the Regularized Benamou-Brenier method with different β values and varying levels of discretization dt and dx.

2.1.3. *Geodesic.* The last technique we present is based on the recent work by Cui et al. [6]. The technique is based on a reformulation of the Benamou-Brenier problem (3) posed in $\mathbb{R}^d$; see Remark 1.1. The authors of [6] reformulate the problem as the Hamiltonian PDE system

$$\begin{aligned} &\frac{\partial \rho(t,x)}{\partial t} + \nabla \cdot (\rho(t,x) \nabla S(t,x)) = 0 \\ &\frac{\partial S(t,x)}{\partial t} + \frac{1}{2} ||\nabla S(t,x)||^2 = 0 \\ &\rho(0,x) = \rho_0(x) \ , \quad \rho(1,x) = \rho_1(x) \ , \end{aligned} \tag{7}$$

where $\nabla S = v$. Here, the Hamiltonian is given by $H(\rho, S) = \frac{1}{2} \int_{\mathbb{R}^d} \|\nabla S\|^2 \rho dx$. When the reformulation holds (see [6]), then, if $S(0,x)$ is known, for the Wasserstein distance the equality $g_W(\rho_0, \rho_1) = \sqrt{2H(\rho_0(x), S(0,x))}$ holds as well. Furthermore, the optimal map has the form $T(x) = x + v(0,x)$. The basic idea of [6] is to find an initial $S(0,x)$ (or $v(0,x)$) such that the trajectory starting at $(\rho_0, S(0,x))$ arrives at ρ_1 at $t = 1$. This is the well-known *geodesic equation* between the two densities ρ_0 and ρ_1 on the Wasserstein manifold (see [25]). But, since S is defined only up to an arbitrary constant, the boundary value problem (7) cannot have a unique solution. Because of this fact, we end up (just like the authors of [6] did, albeit at the discrete level) using the formulation based on ρ and

v:

$$\begin{aligned} &\frac{\partial \rho(t,x)}{\partial t} + \nabla \cdot (\rho(t,x) v(t,x)) = 0 \\ &\frac{\partial v(t,x)}{\partial t} + \frac{1}{2}\nabla ||v(t,x)||^2 = 0 \\ &\rho(0,x) = \rho_0(x) \ , \quad \rho(1,x) = \rho_1(x) \ . \end{aligned} \tag{8}$$

As far as the Wasserstein distance is concerned, one can obtain it from the square root of

$$\int_{\mathbb{R}^d} \|v(0,x)\|^2 \rho_0(x) dx \ . \tag{9}$$

2.2. **Numerical Implementation.** In this Section, we discuss some implementation issues of the basic algorithms from Section 2.1.

Restriction 2.1. *We will consider two types of problems. (a) Periodic problems, which are naturally formulated on the torus, and (b) Problems given on finite rectangular domains: $\Omega = [a_0, a_1] \times [b_0, b_1]$; furthermore, for convenience, we also assume that $(b_1 - b_0)$ and $(a_1 - a_0)$ are rationally related, that is there are $p, q \in \mathbb{N}$ such that $p(a_1 - a_0) = q(b_1 - b_0)$.*[2] *In fact, we could also consider two different rectangular domains for the two different densities, say $X = [a_0, a_1] \times [b_0, b_1]$ for ρ_0 and $Y = [\alpha_0, \alpha_1] \times [\beta_0, \beta_1]$ for ρ_1, but it is a simple linear change of variable to reduce Y to X.*

Remark 2.2. *Note that consideration of a finite rectangular domain poses some nontrivial restrictions on the approach of Section 2.1.3. In particular, the formulation based on* (8) *of [6] on a finite domain Ω imposes zero-flux conditions, more specifically homogeneous boundary conditions for v and homogeneuous Neumann conditions for $\rho(t,x)$: $v = 0$ and $\frac{\partial \rho}{\partial n} = 0$ on $\partial\Omega$ (here, n is the outer normal). If these are severely violated, the use of this approach on a truncated domain is of dubious value.*

2.2.1. *Monge-Ampere Discretization.* As mentioned in Section 2.1.1, we follow the approach of [9] for discretizing (2).

The first thing to decide is how to choose the orthonormal vectors in the monotóne discretization of the derivatives (see (4)). Rather than considering all possible orthonormal bases of $\mathbb{R}^2$,we restrict the set V of (4) to these two bases:

$$\{\widetilde{v}_1, \widetilde{v}_2\} = \left\{ \begin{pmatrix} 1 \\ 0 \end{pmatrix}, \begin{pmatrix} 0 \\ 1 \end{pmatrix} \right\}, \quad \{\widehat{v}_1, \widehat{v}_2\} = \left\{ \frac{1}{\sqrt{2}} \begin{pmatrix} 1 \\ 1 \end{pmatrix}, \frac{1}{\sqrt{2}} \begin{pmatrix} 1 \\ -1 \end{pmatrix} \right\}$$

Using these sets, we derived centered difference formulas for both first and second derivatives. (The first derivatives of course are needed to evaluate $\rho_1(\nabla u)$.) For example, for the first derivatives we have

$$\begin{aligned} [D_{\widetilde{v}_1} u]_{ij} &= \frac{u_{i+1,j} - u_{i-1,j}}{2h}, \quad [D_{\widetilde{v}_2} u]_{ij} = \frac{u_{i,j+1} - u_{i,j-1}}{2h}, \\ [D_{\widehat{v}_1} u]_{ij} &= \frac{u_{i+1,j+1} - u_{i-1,j-1}}{2\sqrt{2}h}, \quad [D_{\widehat{v}_2} u]_{ij} = \frac{u_{i,+1,j-1} - u_{i-1,j+1}}{2\sqrt{2}h}. \end{aligned}$$

where h is the mesh size of the grid (recall that we can take same mesh-size in both coordinate direction). Similarly for the second derivative approximations (see [9]).

[2]Note that this assumption allows us to restrict consideration to discretizations having the same mesh-size in both x_1 and x_2 directions.

The second key aspect of the algorithm is how to select the boundary conditions. For periodic problems, we cannot use (2) as given, since there cannot be any periodic convex function u (except the constants) satisfying $\rho_1 \det D^2 u = \rho_0$ with ρ_0 and ρ_1 periodic. The appropriate setup now is not for u to be convex but rather $\frac{1}{2}\|x\|^2 - u$ to be (e.g., see [16] and [23, pp. 211–214]), so that the the optimal map will be its gradient, that is $T(x) = x - \nabla u(x)$ (in the periodic sense), and now u satisfies this Monge-Ampere PDE:

$$\rho_1 (x - \nabla u) \det(I - D^2 u) \;=\; \rho_0(x) \;. \tag{10}$$

For rectangular domains, we followed the approach of [9] and implemented the so-called *transport boundary conditions*: "The gradient of u maps the boundary onto the boundary". That is:

$$\nabla u(\partial\Omega) = \partial\Omega \;. \tag{11}$$

These are particularly easy to implement when we have two rectangular regions (in fact, for more general polygonal regions as well) $X = [a_0, a_1] \times [b_0, b_1]$ and $Y = [\alpha_0, \alpha_1] \times [\beta_0, \beta_1]$. Then (11) become:

$$\begin{aligned} &u_{x_1}(a_0, x_2) = \alpha_0,\ \forall x_2 \in [b_0, b_1], \quad u_{x_1}(a_1, x_2) = \alpha_1,\ \forall x_2 \in [b_0, b_1], \\ &u_{x_2}(x_1, b_0) = \beta_0,\ \forall x_1 \in [a_0, a_1], \quad u_{x_2}(x_1, b_1) = \beta_1,\ \forall x_2 \in [a_0, a_1]. \end{aligned} \tag{12}$$

Let h be the mesh size of the $N \times M$ grid, such that $(x_1)_1 = a_0$, $(x_1)_N = a_1$, $(x_2)_1 = b_0$, and $(x_2)_M = b_1$. Then (12) are discretized as:

$$\begin{aligned} &\frac{u_{3,j} - u_{1,j}}{2h} = \alpha_0,\ \forall j \in [2, M-1], \quad \frac{u_{N,j} - u_{N-2,j}}{2h} = \alpha_1,\ \forall j \in [2, M-1], \\ &\frac{u_{i,3} - u_{i,1}}{2h} = \beta_0,\ \forall i \in [2, N-1], \quad \frac{u_{i,M} - u_{i,M-2}}{2h} = \beta_1,\ \forall i \in [2, N-1], \end{aligned}$$

and at the corners:

$$\begin{aligned} &\frac{u_{3,3} - u_{1,1}}{2\sqrt{2}h} = \frac{\alpha_0 + \beta_0}{\sqrt{2}}, \quad \frac{u_{N,1} - u_{N-2,3}}{2\sqrt{2}h} = \frac{\alpha_1 - \beta_0}{\sqrt{2}}, \\ &\frac{u_{1,M} - u_{3,M-2}}{2\sqrt{2}h} = \frac{-\alpha_0 + \beta_1}{\sqrt{2}}, \quad \frac{u_{N,M} - u_{N-2,M-2}}{2\sqrt{2}h} = \frac{\alpha_1 + \beta_1}{\sqrt{2}}. \end{aligned}$$

Finally, we add the condition $u_{11} = 0$ to remove the ambiguity resulting from the fact that $u(x)$ is defined only up to a constant.

Remark 2.3. *To be able to handle non-polygonal domains X and Y, in [2] the authors proposed to use boundary conditions inherited from the signed distance function $\sigma(\nabla u(x))$:*

$$\sigma(\nabla u(x)) = \mathit{dist}(\nabla u(x), \partial Y) = 0,\ \forall x \in \partial X.$$

Unfortunately, we were not successful in implementing this type of boundary conditions and to replicate the results of [2].

Once the previous discretization is adopted, the Monge-Ampére PDE is replaced by its difference analog and the discretized system is solved using Newton's method. As usual, for Newton's method it is important to give a good initial guess. To this end, we experimented with three different approaches.

Initial Guess for Newton.

(i) *Trivial.* Here we use the identity as the approximation to the optimal map, that is $u(x) = \frac{1}{2}\|x\|^2$.

(ii) *Interpolation.* We interpolate a solution obtained on a coarse grid to obtain an initial guess for the fine grid. In other words, assuming that N and M are both even, the initial guess u^0 on the $N \times M$ grid is the solution u^* defined on the $\frac{N}{2} \times \frac{M}{2}$ grid, which is interpolated on the $N \times M$ grid (we used the `MATLAB` built-in function `interp2` which does linear interpolation). This is done recursively (for as long as division by 2 returns an integer answer) until $\max N, M \leq 8$. Finally, for the coarsest grid we used the identity map as an initial guess.

(iii) *Homotopy.* Here, let $X = Y$. We introduce an artificial source probability density $\widetilde{\rho}_0(\mu, x)$:

$$\widetilde{\rho}_0(\mu, x) = (1 - \mu)\rho_1(x) + \mu\rho_0(x)$$

and transport $\widetilde{\rho}_0$ to ρ_1 as μ goes from zero to one. At $\mu = 0$ we are mapping ρ_1 to ρ_1, which corresponds to the identity mapping. We begin with $\Delta^0 = 1/10$ or $1/100$ and update it based on the number of Newton iterations in the previous step:

$$\Delta^i = 2^{\frac{4-k}{3}}\Delta^{i-1}, \quad \mu^i = \mu^{i-1} + \Delta^i$$

where k is the number of Newton iterations required to solve problem at μ^{i-1}.

The results of Table 2 compare performance of the above different options to initialize Newton's method, and they are typical, showing that in the end the simplest option of using the trivial initial guess is also the most efficient. Of course, in all cases the same solution was recovered.

	Identity		**Interpolation**		**Homotopy**	
dx	**Newton**	**Time**	**Newton**	**Time**	**Nsteps, Newton**	**Time**
Problem 4.9						
$\frac{1}{8}$	6	0.01	6	0.03	12, 50	0.05
$\frac{1}{16}$	6	0.02	10	0.05	16, 66	0.18
$\frac{1}{32}$	8	0.19	12	0.34	15, 62	1.47
$\frac{1}{64}$	9	2.78	16	5.25	15, 62	20.2
$\frac{1}{128}$	17	78.3	21	101	13 ,54	262
Problem 4.10						
$\frac{1}{8}$	7	0.23	7	0.19	3, 20	0.06
$\frac{1}{16}$	6	0.50	7	0.66	5, 40	0.16
$\frac{1}{32}$	6	1.91	11	2.65	7, 60	1.60
$\frac{1}{64}$	8	9.17	15	13.8	7, 61	22.1
$\frac{1}{128}$	12	81.9	14	104	4, 32	281

TABLE 2. Total number of Newton's iterations, number of homotopy steps if applicable, and execution times, when the nonlinear Monge-Ampére discretization is solved with different initial guesses for Newton's method.

2.2.2. *Regularized Benamou-Brenier Discretization.* Here, we need to solve problem (6) by discretizing it on a spatial and temporal grid. Note that the dependence of the discretized constraints on $\widetilde{m}$ and ρ is linear when standard finite difference schemes are used for derivative approximations. This method is well suited for rectangular domains, but not when we pose the problem on the torus (periodic problems), because of the requirement of 0-flux on m.

Under Restriction 2.1, let the domain $\Omega = [a_0, a_1] \times [b_0, b_1]$ be discretized with a uniform meshsize h such that $(x_1)_i = a_0 + h(i-1)$, $i = 1, 2, \ldots, N$, $(x_2)_j = b_0 + h(j-1)$, $j = 1, 2, \ldots, M$. In addition, let L be the number of internal time values such that $t_l = ldt$, $l = 0, 1, \ldots, L+1$ and $dt = \frac{1}{L+1}$. The probability density values $\rho(t_l, (x_1)_i, (x_2)_j)$ are defined on the grid vertices and $\widetilde{m}(t_l, (x_1)_{i+0.5}, (x_2)_{j+0.5})$ are defined on the grid edges. Then, the discretization of (6) is:

$$\begin{aligned} &\min_U f(U) \\ &\text{s. t. } AU = b \end{aligned} \tag{13}$$

where $U = \begin{pmatrix} m^{x_1}(:) \\ m^{x_2}(:) \\ R(:) \end{pmatrix} \in \mathbb{R}^{((N-1)M+N(M-1))(L+1)+LNM}$ represent the grid analog comprising the two components of $\widetilde{m}$ and of ρ and we need to impose/maintain positivity of R.

So, $m^{x_1} \in \mathbb{R}^{(N-1)\times M\times(L+1)}$, $m^{x_2} \in \mathbb{R}^{N\times(M-1)\times(L+1)}$, $R \in \mathbb{R}^{N\times M\times L}$, and the objective function $f(U)$ is given by

$$\begin{aligned} &f(U) = f(m^{x_1}, m^{x_2}, R) = \\ &= \sum_{l=0}^{L}\sum_{i=1}^{N-1}\sum_{j=1}^{M-2} \frac{2(m^{x_1}_{i+0.5,j,l})^2}{\rho_{i,j,l}+\rho_{i+1,j,l}} + \frac{\beta^2}{h^2}(\log(\rho_{i,j,l}) - \log(\rho_{i+1,j,l}))^2 \frac{\rho_{i,j,l}+\rho_{i+1,j,l}}{2} + \\ &+ \sum_{l=0}^{L}\sum_{i=1}^{N-2}\sum_{j=1}^{M-1} \frac{2(m^{x_2}_{i,j+0.5,l})^2}{\rho_{i,j,l}+\rho_{i,j+1,l}} + \frac{\beta^2}{h^2}(\log(\rho_{i,j,l}) - \log(\rho_{i,j+1,l}))^2 \frac{\rho_{i,j,l}+\rho_{i,j+1,l}}{2} \end{aligned} \tag{14}$$

and $A \in \mathbb{R}^{((L+1)NM+L)\times(((N-1)M+N(M-1))(L+1)+LNM)}$ and $b \in \mathbb{R}^{(L+1)NM+L}$ are obtained from the constraints:

$$\begin{aligned} &\frac{\rho_{i,j,l+1}-\rho_{i,j,l}}{dt} + \frac{1}{h}((m^{x_1}_{i+0.5,j,l} - m^{x_1}_{i-0.5,j,l}) + (m^{x_2}_{i,j+0.5,l} - m^{x_2}_{i,j-0.5,l})) = 0 \\ &i = 1, 2, \ldots, N; \qquad j = 1, 2, \ldots, M; \qquad l = 0, 1, 2, \ldots, L \\ &\sum_{i=1}^{N}\sum_{j=1}^{M} \rho_{i,j,l} = 1 \qquad l = 1, 2, \ldots, L \end{aligned} \tag{15}$$

and the zero flux condition is used for ghost cells: $m^{x_1}_{0.5,j,l} = m^{x_1}_{N+0.5,j,l} = 0$ and $m^{x_2}_{i,0.5,l} = m^{x_2}_{i,M+0.5,l} = 0$. Then, we solve the discrete minimization problem (13) by moving from the current iterate in the direction of the best quadratic approximation (a modified Newton's method) subject to linear constraints and positivity constraints on the components R of U (cfr. with [14]):

$$U^{k+1} = U^k + \alpha d^k \ , \ R^{k+1} > 0 \ , \tag{16}$$

where

$$\begin{aligned} &d^k = \arg\min_d d^T \nabla f(U^k) + \frac{1}{2} d^T H(u^k) d \\ &\text{s.t. } Ad = 0 \ , \end{aligned} \tag{17}$$

where $\nabla f(u)$ and $H(u)$ are the gradient and the Hessian of $f(u)$, respectively. This is a classic quadratic minimization problem for d in the kernel of A, subject to positivity constraints on the subset of the variables associated to R. We solve this problem in three steps: (i) First we find an orthonormal basis for the kernel of A, call W its matrix representation; then (ii) we write $d = Wc$ for some c; (iii) finally, we reformulate the minimization problem for c, by requiring positivity of the relevant variables. We solve this last problem by the tried and true `MATLAB` function `quadprog`. Finally, we refer to Section 4 for the values of α in (16) that we used in practice.

2.2.3. *Geodesic discretization: Multiple shooting method.* The authors of [6] provided a `Matlab` code on `github` implementing a multiple shooting approach to solve the discretized version of (7)-(8), for both 1-d and 2-d. We have used their code in our 2-d experiments, as well as implemented our own versions for 1-d problems.

For completeness, we next describe our discretization for $\rho(t,x)$ and $v(t,x)$. Let the domain $X = Y = [a_0, a_1]$ be discretized by a uniform mesh of n points with spacing dx, and let L be the number of internal time points with spacing $dt = \frac{1}{L+1}$. Density values $\rho(t_l, x_i)$ are defined on grid points and $v(t_l, x_{i+0.5})$ are defined on the grid edges.

Then, the discretized problem (8) can be formulated as:

$$\frac{\rho_{i,l+1} - \rho_{i,l}}{dt} + \rho_{i,l}\frac{\nu_{i+0.5,l} - \nu_{i-0.5,l}}{dx} + \frac{v_{i+0.5,l} + v_{i-0.5,l}}{2} \cdot \frac{\rho_{i+1,l} - \rho_{i-1,l}}{2dx} = 0, \quad i = 1, 2, \ldots, n$$

$$\frac{v_{i+0.5,l+1} - v_{i+0.5,l}}{dt} + v_{i+0.5,l}\frac{v_{i+1.5} - v_{i-0.5}}{2dx} = 0, \quad i = 1, 2, \ldots, n-1$$

where $l = 0, 1, \ldots, L$. For periodic boundary conditions, we then impose

$$\rho_{-1,l} = \rho_{n-1,l}\ , \quad \rho_{n+1,l} = \rho_{2,l}\ , \quad l = 0, 1, \ldots, L$$

Instead, zero flux condition on $v(x,t)$ and homogeneous Neumann conditions on $\rho(x,t)$ give

$$v_{0.5,l} = v_{n+0.5,l} = 0, \quad l = 0, 1, \ldots, L$$

$$\frac{\rho_{2,l} - \rho_{-1,l}}{2dx} = \frac{\rho_{n+1,l} - \rho_{n-1,l}}{2dx} = 0, \quad l = 0, 1, \ldots, L$$

Remark 2.4 (Wasserstein distance approximation)**.** *In the fluid-flow formulation, the minimum value of* (3) *gives $g_W^2(\rho_0, \rho_1)$, the square of the Wasserstein distance between ρ_0 and ρ_1. To obtain this distance when we have just the optimal map (say, by solving the Monge-Ampére PDE), one needs to approximate the integral below*

$$g_W^2 = \int_\Omega \|T(x) - x\|^2 \rho_0(x) dx\ , \tag{18}$$

and approximating this integral on the grid where we have solved for $T(x)$ renders an approximation scheme for g_W^2. Of course, this is also a very inexpensive procedure once $T(x)$ is known.

Remark 2.5. *Ideally, the two different fluid-flow formulations that we considered, that based on* (5) *and that based on* (8) *, should recover the same geodesic trajectory from ρ_0 to ρ_1. However, in general, this is not borne out in practice, well beyond the discretization error level; e.g., see Figure 1 for a plot of the (sup-norm of the) difference between the two trajectories obtained by the two different methods. This discrepancy highlights the need to make sure that the assumptions underlying validity of different formulations are satisfied.*

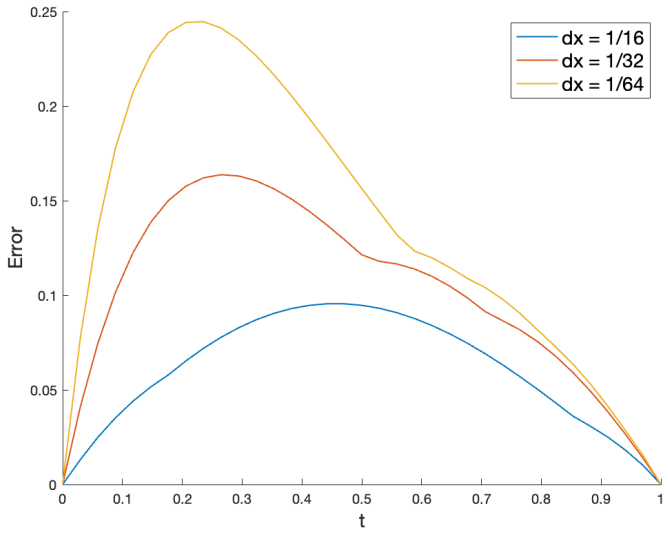

FIGURE 1. Sup-norm of the difference on the grid between $\rho(t,x)$ obtained by the techniques based on (6) (with $\beta = 10^{-5}$) and (7) on Problem 4.2.

2.3. **Hybrid technique: From $v(0,x)$ to the full geodesic evolution.** One more method with which we have experimented rests on a very natural idea. Suppose we are able, for example by exploiting separability (see Section 3 and especially Section 3.3.1), to obtain the initial velocity $v(0,x)$ in the fluid-flow formulation. Then, we can approximate the geodesic by solving the PDE system (7), with no need to iterate to find the correct initial velocity. The resulting hybrid method allows to obtain the full evolution of the density without the need to solve a nonlinear problem to get the correct initial velocity. For example, the density evolution of Figure 5 was obtained using this hybrid technique, with the initial velocity obtained from the approach in Section 3.3.1. In principle, for as long as the conditions relating the optimal map T to the initial velocity $v(0,x)$ hold, namely $T(x) = x + v(0,x)$, then one may obtain the initial velocity also from the solution of the Monge-Ampére PDE, that is from T; the advantage of this point of view is that it applies even if the problem is not separable.

3. Separable Class of OT Problems

As it turns out, many of the problems that arise in the study of optimal transport are of a special type, which we will call *separable*, in analogy to the technique of separation of variables commonly performed for PDEs. To witness, examples of separable problems are in the works [6, 9, 14], and in fact the common case of Gaussian distributions ρ_0 and ρ_1 with diagonal covariance matrices (or with covariance matrices simultaneously diagonalizable), as well as the case of uniform distribution, are all separable. Below, for these separable problems we will give some new theoretical results and devise much more accurate and efficient versions of the previously examined numerical techniques, specifically for the solution of the Monge-Ampére PDE. By contrast, in the above cited works, the separability of the OT problems was neither recognized nor exploited.

3.1. **Separation Process.** We describe the process on rectangular domains, but with minimal changes everything carries over to $\mathbb{R}^d$ or $\mathbb{T}^p$. Let the rectangular domains of $\rho_0(x)$ and $\rho_1(y)$ be $X = [a_0, a_1] \times [b_0, b_1]$ and $Y = [\alpha_0, \alpha_1] \times [\beta_0, \beta_1]$.

Definition 3.1. *We say that the pair of positive probability densities ρ_0 and ρ_1 is a* separable pair of densities *on X, respectively Y, if*

$$\rho_0(x) = R_1(x_1)R_2(x_2), \;\; x \in X, \quad \rho_1(y) = S_1(y_1)S_2(y_2), \;\; y \in Y. \tag{19}$$

Equivalently, we will just say that ρ_0 and ρ_1 are separable.

Lemma 3.2. *Let ρ_0 and ρ_1 be a separable pair of densities as in Definition 3.1. Then, we can always assume that*

$$\begin{aligned} &R_1(x_1) > 0, \quad \int_{a_0}^{a_1} R_1(x_1)dx_1 = 1, \quad R_2(x_2) > 0, \quad \int_{b_0}^{b_1} R_2(x_2)dx_2 = 1, \\ &S_1(y_1) > 0, \quad \int_{\alpha_0}^{\alpha_1} S_1(y_1)dy_1 = 1, \quad S_2(y_2) > 0, \quad \int_{\beta_0}^{\beta_1} S_2(y_2)dy_2 = 1. \end{aligned} \tag{20}$$

Proof. The claim follows from the fact that $\rho_0(x_1, x_2)$ and $\rho_1(y_1, y_2)$ are probability densities and therefore:

$$1 = \int_{b_0}^{b_1}\int_{a_0}^{a_1} \rho_0(x_1, x_2)dx_1dx_2 = \int_{b_0}^{b_1}\int_{a_0}^{a_1} R_1(x_1)R_2(x_2)dx_1dx_2 = \int_{b_0}^{b_1}\int_{a_0}^{a_1} \frac{m}{m}R_1(x_1)R_2(x_2)dx_1dx_2$$

$$1 = \int_{b_0}^{b_1}\int_{a_0}^{a_1} mR_1(x_1)\frac{1}{m}R_2(x_2)dx_1dx_2 = \left[\int_{a_0}^{a_1} mR_1(x_1)dx_1\right]\left[\int_{b_0}^{b_1} \frac{1}{m}R_2(x_2)dx_2\right]$$

$$1 = \int_{\beta_0}^{\beta_1}\int_{\alpha_0}^{\alpha_1} \rho_1(y_1, y_2)dy_1dy_2 = \int_{\beta_0}^{\beta_1}\int_{\alpha_0}^{\alpha_1} S_1(y_1)S_2(y_2)dy_1dy_2 = \int_{\beta_0}^{\beta_1}\int_{\alpha_0}^{\alpha_1} \frac{n}{n}S_1(y_1)S_2(y_2)dy_1dy_2$$

$$1 = \int_{\beta_0}^{\beta_1}\int_{\alpha_0}^{\alpha_1} \frac{1}{n}S_1(y_1)nS_2(y_2)dy_1dy_2 = \left[\int_{\alpha_0}^{\alpha_1} \frac{1}{n}S_1(y_1)dy_1\right]\left[\int_{\beta_0}^{\beta_1} nS_2(y_2)dy_2\right]$$

for some constants m and n. Therefore, we can always renormalize R_1, R_2, S_1 and S_2, as stated in (20). □

Next, we look at the implication of having separable densities on the two formulation considered in this work: the Monge Ampére PDE and the Benamou-Brenier formulation.

3.2. **Separable Monge-Ampére.** Recall that, on the rectangular domains X and Y, we need to solve the following problem for positive ρ_0 and ρ_1:

$$\begin{aligned} &\det\left(D^2u(x)\right) = \frac{\rho_0(x)}{\rho_1(\nabla u(x))} \\ &u_{x_1}(a_0, x_2) = \alpha_0, \; \forall x_2 \in [b_0, b_1], \quad u_{x_1}(a_1, x_2) = \alpha_1, \; \forall x_2 \in [b_0, b_1], \\ &u_{x_2}(x_1, b_0) = \beta_0, \; \forall x_1 \in [a_0, a_1], \quad u_{x_1}(x_1, b_1) = \beta_1, \; \forall x_2 \in [a_0, a_1], \end{aligned} \tag{21}$$

and that the solution $u(x)$ is unique, up to a constant.

Theorem 3.3. *Let ρ_0 and ρ_1 be separable densities as in Definition 3.1. Then, the 2-d Monge-Ampére problem* (21) *can be reduced to the two 1-d Monge-Ampére problems* (22)*.*

Proof. Since the densities are separable, we seek a solution of (21) of the form $u(x) = u_1(x_1) + u_2(x_2)$. If so, the BCs in (21) rewrite as

$$u_1'(a_0) = \alpha_0, \;\; u_1'(a_1) = \alpha_1, \;\; u_2'(b_0) = \beta_0, \;\; u_2'(b_1) = \beta_1.$$

The differential part of (21) rewrites as

$$\det(D^2u(x_1,x_2)) = u_{x_1x_1}u_{x_2x_2} - u_{x_1x_2}^2 = \frac{\rho_0(x_1,x_2)}{\rho_1(u_{x_1},u_{x_2})} \iff u_1''(x_1)u_2''(x_2) = \frac{R_1(x_1)R_2(x_2)}{T_1(u_1'(x_1))T_2(u_2'(x_2))}$$

which we can formally rewrite as

$$\frac{u_1''(x_1)S_1(u_1'(x_1))}{R_1(x_1)} = \frac{R_2(x_2)}{u_2''(x_2)S_2(u_2'(x_2))} = c \neq 0$$

where c is some constant (this is because the left, respectively right, hand sides above is a function only of x_1, respectively of x_2), and R_1, R_2, S_1, S_2, are normalized as in Lemma 3.2. By selecting the constant $c = 1$, we get

$$u_1''(x_1) = \frac{R_1(x_1)}{S_1(u_1'(x_1))}, \quad u_2''(x_2) = \frac{R_2(x_2)}{S_2(u_2'(x_2))} \; .$$

As a result, we obtain the two 1-d Monge-Ampere equations:

$$\begin{aligned} &S_1(u_1'(x_1))u_1''(x_1) = R_1(x_1), \quad u_1'(a_0) = \alpha_0, \quad u_1'(a_1) = \alpha_1 \\ &S_2(u_2'(x_2))u_2''(x_2) = R_2(x_2), \quad u_2'(b_0) = \beta_0, \quad u_2'(b_1) = \beta_1. \end{aligned} \tag{22}$$

In conclusion, we can take the solution $u(x)$ of (21) given by the representation $u(x) = u_1(x_1) + u_2(x_2)$ with u_1 and u_2 satisfying (22). □

Corollary 3.4. *Under the conditions of Theorem 3.3, the unique optimal map $T(x) = \nabla u(x)$ rewrites as*

$$T(x) = \begin{bmatrix} T_1(x_1) \\ T_2(x_2) \end{bmatrix} = \begin{bmatrix} {u_1}'(x_1) \\ {u_2}'(x_2) \end{bmatrix} \tag{23}$$

where u_1 and u_2 solve (22).

Moreover, the Wasserstein distances enjoy a separability result as well:

$$g_W^2(\rho_0,\rho_1) = g_W^2(R_1,S_1) + g_W^2(R_2,S_2) \; . \tag{24}$$

Proof. The rewriting (23) is immediate from Theorem 3.3. The result on the Wasserstein distance comes from the following reasoning. We have

$$\begin{aligned} &\int_X \|x - T(x)\|^2 \rho_0(x)dx = \int_{x_1=a_0}^{a_1}\int_{x_2=b_0}^{b_1} \| \begin{bmatrix} x_1 - T_1(x_1) \\ x_2 - T_2(x_2) \end{bmatrix} \|^2 \; R_1(x_1)R_2(x_2)dx_2dx_1 \\ &= \int_{x_1=a_0}^{a_1}\int_{x_2=b_0}^{b_1} \left[(x_1 - T_1(x_1))^2 + (x_2 - T_2(x_2))^2\right] R_1(x_1)R_2(x_2)dx_1dx_2 \\ &= \int_{a_0}^{a_1}\int_{b_0}^{b_1} R_2(x_2)dx_2(x_1 - T_1(x_1))^2R_1(x_1)dx_1 + \int_{b_0}^{b_1}\int_{a_0}^{a_1} R_1(x_1)dx_1(x_2 - T_2(x_2))^2R_2(x_2)dx_2 \\ &= \int_{a_0}^{a_1}(x_1 - T_1(x_1))^2R_1(x_1)dx_1 + \int_{b_0}^{b_1}(x_2 - T_2(x_2))^2R_2(x_2)dx_2 \end{aligned}$$

and the result follows. □

Remark 3.5. *The result on separability of the Wasserstein distance is consistent with the result in [15], where the authors consider a restricted class of separable densities and in [15, Proposition 5] provide separability result for the "Wasserstein Information Matrix", and further in [15, Equation (2)] relate the Wasserstein distance to the Wasserstein Information Matrix.*

We reiterate that when the domains of ρ_0 and ρ_1 are rectangles, and the probability densities form a separable pair, it is possible to simplify the task of solving the original 2-d Monge-Ampére problem by solving two 1-d problems.

We refer to the Appendix at the end of the present paper for a result showing that (22) is well posed in the sense of Hadamard. This will imply that it must be possible to devise robust numerical methods for its solution, and hence for solving the Monge-Ampére equation (21) relative to separable densities.

3.3. **Separable Densities with Benamou-Brenier Formulation.** Here we discuss the impact of having a separable density pair with respect to the Benamou-Brenier formulation (3).

Definition 3.6. *We say that the velocity field $v(t,x)$ in* (3) *is* separable *if it has the form $v(t,x) = \begin{bmatrix} v_1(t,x_1) \\ v_2(t,x_2) \end{bmatrix}$ for all (t,x_1,x_2). Similarly, we say that the density $\rho(t,x)$ is separable if it can be written as product of 1-d densities: $\rho(t,x) = R_1(t,x_1)R_2(t,x_2)$.*

Lemma 3.7. *Let ρ_0 and ρ_1 be separable densities as in Definition 3.1. Then, the velocity field at $t=0$, $v^0(x) = v(0,x)$, is separable.*

Proof. This is a consequence of the relation between the optimal map $T(x_1,x_2)$ and the velocity field $v(t,x_1,x_2)$:

$$T(x_1,x_2) = \begin{pmatrix} x_1 \\ x_2 \end{pmatrix} + v(0,x_1,x_2) = \begin{pmatrix} x_1 \\ x_2 \end{pmatrix} + \begin{bmatrix} v_1(0,x_1,x_2) \\ v_2(0,x_1,x_2) \end{bmatrix}.$$

Therefore, as a consequence of Corollary 3.4, the initial velocity field is separable:

$$v(0,x_1,x_2) = \begin{bmatrix} v_1^0(x_1) \\ v_2^0(x_2) \end{bmatrix}.$$

□

Theorem 3.8. *Let ρ_0 and ρ_1 be separable densities as in Definition 3.1. Consider the formulation (8) of the OT problem. Then, the velocity field is separable for all $t \in [0,1]$: $v(t,x) = \begin{bmatrix} v_1(t,x_1) \\ v_2(t,x_2) \end{bmatrix}$.*

Proof. Using the Benamou-Brenier formulation (8) the velocity field can be found by solving the PDE

$$\frac{\partial v(t,x)}{\partial t} + \nabla(\frac{1}{2}||v(t,x)||^2) = 0. \tag{25}$$

Writing

$$v(t,x_1,x_2) = \begin{pmatrix} v_1(t,x_1,x_2) \\ v_2(t,x_1,x_2) \end{pmatrix},$$

(25) can be explicitly rewritten as

$$\begin{pmatrix} \frac{\partial v_1(t,x_1,x_2)}{\partial t} \\ \frac{\partial v_2(t,x_1,x_2)}{\partial t} \end{pmatrix} + \begin{pmatrix} \frac{\partial v_1(t,x_1,x_2)}{\partial x_1} v_1(t,x_1,x_2) + \frac{\partial v_2(t,x_1,x_2)}{\partial x_1} v_2(t,x_1,x_2) \\ \frac{\partial v_1(t,x_1,x_2)}{\partial x_2} v_1(t,x_1,x_2) + \frac{\partial v_2(t,x_1,x_2)}{\partial x_2} v_2(t,x_1,x_2) \end{pmatrix} = 0$$

Now, from Lemma 3.7 we know that the velocity field is separable at $t = 0$: $v(0, x_1, x_2) = \begin{bmatrix} v_1^0(x_1) \\ v_2^0(x_2) \end{bmatrix}$. But then, the evolution in time of v will preserve this property. This is a consequence of the fact that the derivative at $t = 0$ of $v(t, x)$ is separable. In fact, from (25) one has that

$$\left[\frac{\partial}{\partial t} v(t, x_1, x_2)\right]_{t=0} = -\begin{pmatrix} \frac{\partial v_1(0,x_1,x_2)}{\partial x_1} v_1(0, x_1, x_2) + \frac{\partial v_2(0,x_1,x_2)}{\partial x_1} v_2(0, x_1, x_2) \\ \frac{\partial v_1(0,x_1,x_2)}{\partial x_2} v_1(0, x_1, x_2) + \frac{\partial v_2(0,x_1,x_2)}{\partial x_2} v_2(0, x_1, x_2) \end{pmatrix}$$

that is, using Lemma 3.7:

$$\left[\frac{\partial}{\partial t} v(t, x_1, x_2)\right]_{t=0} = -\begin{pmatrix} (\partial_{x_1} v_1^0(x_1)) v_1^0(x_1) \\ (\partial_{x_2} v_2^0(x_2)) v_2^0(x_2) \end{pmatrix}$$

and thus

$$\begin{pmatrix} \frac{\partial}{\partial t} v_1(t, x_1) \\ \frac{\partial}{\partial t} v_2(t, x_2) \end{pmatrix} = -\begin{pmatrix} (\partial_{x_1} v_1(t, x_1)) v_1(t, x_1) \\ (\partial_{x_2} v_2(t, x_2)) v_2(t, x_2) \end{pmatrix} . \tag{26}$$

□

Remark 3.9. [Is $\rho(t, x)$ separable?] *Under the same conditions of Theorem 3.8, it is unclear whether the probability density $\rho(t, x_1, x_2)$ is separable for all t, even when at times $t = 0$ and $t = 1$ one has a separable pair. That is, if $\rho(0, x_1, x_2) = R_1(x_1)R_2(x_2)$ and $\rho(1, x_1, x_2) = S_1(x_1)S_2(x_2)$, can we conclude that $\rho(t, x_1, x_2) = R_1(t, x_1)R_2(t, x_2)$ for all $t \in (0, 1)$? In general, this is not clear to us. However, we point out that in order for it to be true then one would need the following to hold (using Theorem 3.8)*

$$\begin{aligned} \frac{\partial}{\partial t} R_1(t, x_1) + \frac{\partial}{\partial x}(v_1(t, x_1) R_1(t, x_1)) = 0 \\ \frac{\partial}{\partial t} R_2(t, x_2) + \frac{\partial}{\partial x}(v_2(t, x_2) R_2(t, x_2)) = 0 \end{aligned} \tag{27}$$

along with the velocity equations from (26)*. Below, we give some evidence that this fact does not hold, by comparing the solutions obtained by assuming that ρ is separable, and using* (27)*, versus solving the problem for $\rho(t, x)$ without assuming separability of ρ explicitly. As it can be seen from Figure 2, it appears that the density $\rho(t, x)$ is not separable, in general.*

3.3.1. *Fluid-flow, optimal map, separability.* In spite of Remark 3.9, it is still possible to take advantage of separability when using the fluid-flow formulation. In fact, from separability of the Monge-Ampére problem, we know that the optimal $T(x)$ rewrites as $T(x) = \begin{bmatrix} T_1(x_1) \\ T_2(x_2) \end{bmatrix}$, where T_1 (respectively T_2) is the optimal map for the transport from the 1-d density R_1 to S_1 (respectively, R_2 to S_2). Then, one approach is to use the fluid-flow formulation (in either form (5) or (8)) to perform the 1-d transfers from R_1 to S_1 and from R_2 to S_2 to obtain the initial velocity $\begin{bmatrix} v_1(0, x_1) \\ v_2(0, x_2) \end{bmatrix}$. This can then be used to integrate directly for the density evolution, for example integrating (7), but also to approximate the optimal map (for as long as the conditions leading to the equality below hold)

$$T(x) = \begin{bmatrix} T_1(x_1) \\ T_2(x_2) \end{bmatrix} = \begin{bmatrix} x_1 + v_1(0, x_1) \\ x_2 + v_2(0, x_2) \end{bmatrix} .$$

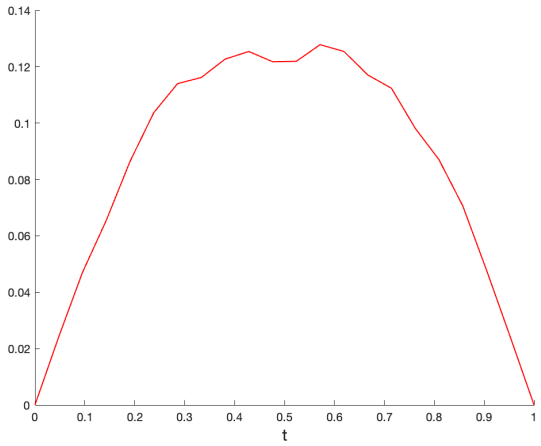

FIGURE 2. Checking separability of $\rho(t,x)$ on Problem 4.8. Sup-norm of the difference on the grid, at different times, between the solutions obtained pretending that ρ is separable, and using (27), and $\rho(t,x)$ obtained by multiple shooting without assuming separability of ρ; here, $dx = \frac{1}{32}$.

We used this approach to approximate the optimal map on all separable 2-d problems in Section 4 when using the methods (6) or (8) based on the fluid-flow formulation, that is solving 1-d problems.

Finally, motivated by the previous discussion on separability, we conclude this Section with some results on the numerical discretization of the 1-d Monge Ampére PDE and on the impact of periodic boundary conditions, also in this 1-d case.

3.4. **Numerical Solution of 1-d Monge Ampére.** As we saw before, the Monge-Ampére equation in 1-d reduces to solving the two-point boundary value problem:

$$\begin{aligned} &\rho_1(y(x))y'(x) = \rho_0(x) \\ &y'(a) = \alpha, \quad y'(b) = \beta \end{aligned} \tag{28}$$

where $y(x) = u'(x)$ and

$$\int_a^b \rho_0(x)dx = \int_\alpha^\beta \rho_1(y)dy = 1$$
$$\rho_0(x) > 0, \forall x \in [a,b] \quad \text{and} \quad \rho_1(y) > 0, \quad \forall y \in [\alpha,\beta]\ .$$

Then one approach to solve this problem is to use the analytical form of the exact solution; see [23, Theorem 2.5], which requires computing cumulative distribution functions after performing separation of variables. A more practical way to solve (28), and the one we adopted in this work, is to discretize by a Runge-Kutta (RK) scheme the scalar ODE (28) with only the initial condition $y'(a) = \alpha$. This way we can recover the terminal condition $y'(b) = \beta$ to any desired accuracy. In our numerical experiments we have used the classical RK4 method to solve (28) as an initial value problem from a to b with a fixed stepsize $h = \frac{b-a}{N+1}$. Finally, since we are using RK4, we enforce the normalization of the values

of $\rho_0(x_i)$ in the following way:

$$\text{let} \quad \gamma = \frac{h}{6}\sum_{i=0}^{N}[\rho_0(x_i) + 4\rho_0(x_i + h/2) + \rho_0(x_{i+1})]$$
$$\text{then renormalize} \quad \rho_0^i = \frac{1}{\gamma}\rho_0(x_i) \ .$$

With the above normalization, the final value y_{N+1} will be accurate to β at $\mathcal{O}(h^4)$.

3.5. **Optimal map on 1-d torus.** For one-dimensional MA problem on the torus, the correct formulation now seeks a convex function of the form $x^2/2 - u$ (see (10)), and the optimal map will be of the form

$$T(x) = x - u'(x)$$

where u satisfies

$$1 - u''(x) = \frac{\rho_0(x)}{\rho_1(x - u'(x))} \ , \quad u(0) = u(1), \tag{29}$$

for $x \in [0, 1]$, mod 1.

To solve (29), we exploit the fact that the solution is unique only up to a constant and so we fix the value $u(0) = 0$, and rewrite (29) as the second-order two-point boundary value problem:

$$\begin{cases} 1 - u''(x) = \frac{\rho_0(x)}{\rho_1(x-u'(x))} \\ u(0) = 0, \quad u(1) = 0 \ . \end{cases} \tag{30}$$

For solving (30) we used a single shooting method, by integrating the initial value problem with initial data $u(0) = 0$, $u'(0) = s$, and seeking (via Newton's method) the correct initial velocity $u'(0)$ so that at the end point we get $u(1) = 0$. This is a standard approach, and in our implementation we carried out the numerical integration of the initial value problem with RK4.

Remark 3.10. *A major simplification, allowing to bypass using single shooting and Newton's method, occurs when $\rho_1(y)$ is uniform (i.e. $\rho_1(y) = 1$). This is because* (30) *rewrites as a first-order scalar initial value problem by letting $y(x) = u'(x)$:*

$$1 - y'(x) = \rho_0(x) \ , \quad y(0) = \int_0^1 R_0(s)ds - \frac{1}{2} \ , \tag{31}$$

where $R_0(x)$ is the cumulative distribution function of $\rho_0(x)$:

$$R_0(x) = \int_0^x \rho_0(s)ds \ .$$

It is simple to justify the initial condition for $y(x)$ in (31) *as follows. Rewrite*

$$u''(x) = 1 - \rho_0(x) \implies u'(x) = x - \int_0^x \rho_0(s)ds + u'(0)$$
$$\implies u(x) = \frac{1}{2}x^2 - \int_0^x R_0(s)ds + xu'(0) + u(0).$$

So, enforcing periodicity condition $u(0) = u(1)$ gives $u'(0) = \int_0^1 R(s)ds - \frac{1}{2}$.

4. Computational Examples and Numerical Results

In this section we will provide the set of problems which we have used to test accuracy and overall performance of our implementation for the numerical methods previously presented. Whenever we have an expression for the optimal map, we will report on the error in approximating it. Likewise, we will report on the value we obtain for the approximation of the Wasserstein distance $g_W(\rho_0, \rho_1)$, by using the three different approaches we implemented: when solving the Monge-Ampére problem, g_W is approximated by (18) as outlined in Remark 2.4, for the fluid-flow implementation of (6) it is approximated by the square root of the value in (6), and for the approach based on the geodesic we take the square root of the value in (9).

For all implementations requiring to solve a nonlinear system, we iterated until either the update in norm was less than a preassigned value `TOL`, or we exceeded `maxit` iterations.

4.1. Problems and Results in 1D.

Below, $X = [a, b]$ and $Y = [\alpha, \beta]$ are the domains of the two densities $\rho_0(x)$ and $\rho_1(y)$.

For these problems, we either have the explicit formula for the optimal map, or we can obtain it implicitly as follows. Since $\rho_1(y)dy = \rho_0(x)dx$, then we get $\int_\alpha^y \rho_1(y)dy = \int_a^x \rho_0(x)dx$ or $R_1(y) = R_0(x)$. So, for any given x, we find $y(x)$ (the optimal map) as the solution of

$$R_1(y(x)) - R_0(x) = 0 \ .$$

To find the root of this equation, we used the routine `fzero` of `Matlab`.

Example 4.1. *This is a problem used to compare the numerical solution of the 1-d MA with the solution of the Benamou-Brenier formulation* (6)*. The formulation* (7) *does not apply here, since the implied BCs do not hold. The densities are linear, and the map can be found easily. We have*

$$X = Y = [0, 1], \ \ \rho_0(x) = \frac{2x+1}{2}, \ \ \rho_1(y) = \frac{3-2y}{2}$$

and the optimal transport map is

$$T(x) = \frac{1}{2}(3 - \sqrt{9 - 4x - 4x^2}) \ .$$

As it can be seen from Table 3, solving the system (13), and exploiting the RK integration for the 1-d Monge-Ampére solution, we recover first and the fourth orders of convergence for the respective methods, as expected. In addition, the execution time of RK4 is very short. Multiple shooting method outputs small error too, which is comparable with Regularized Benamou-Brenier method's error. However, it does not show desired order of convergence. In fairness, Example 4.1 is not one where we expected the method based on (8) to work well, since the implied no-flux BCs do not hold.

Example 4.2. *This is a map from a Gaussian to a two-bumps Gaussian. We have*

$$X = Y = [0, 1], \ \ \rho_0(x) = c_1 e^{-5(x-0.5)^2}, \ \ \rho_1(y) = c_2[e^{-50(y-0.25)^2} + e^{-50(y-0.75)^2}],$$

where c_1 and c_2 are normalization constants.

Table 4 shows numerical results for this example. No method performs well for this problem, and the main culprit appears to be the fact that ρ_1 is near 0 at the endpoints.

	Regularized Benamou-Brenier $dt=\frac{1}{21}$, $\beta=10^{-5}$, $\alpha=0.5$, TOL $=10^{-8}$, maxit $=40$				Multiple Shooting $dt=\frac{1}{128}$, $\Delta t=\frac{dt}{32}$, TOL $=10^{-12}$, maxit $=20$				1-d MA: Explicit RK-4		
dx	Map Error	$g_W(\rho_0,\rho_1)$	Time	Newton	Map Error	$g_W(\rho_0,\rho_1)$	Time	Newton	Map Error	$g_W(\rho_0,\rho_1)$	Time
$\frac{1}{16}$	$3.6022*10^{-2}$	$2.0241*10^{-1}$	4.28	26	$7.0847*10^{-2}$	$2.0644*10^{-1}$	2.36	5	$2.4340*10^{-5}$	$1.7951*10^{-1}$	$6.11*10^{-3}$
$\frac{1}{32}$	$2.0514*10^{-2}$	$1.9079*10^{-1}$	19.9	26	$5.7057*10^{-2}$	$1.9231*10^{-1}$	4.21	5	$2.0546*10^{-6}$	$1.7953*10^{-1}$	$1.69*10^{-3}$
$\frac{1}{64}$	$1.1055*10^{-2}$	$1.8512*10^{-1}$	117	26	$5.0202*10^{-2}$	$1.8529*10^{-1}$	14.1	5	$1.4717*10^{-7}$	$1.7953*10^{-1}$	$1.69*10^{-3}$
$\frac{1}{128}$	$5.7552*10^{-3}$	$1.8232*10^{-1}$	760	26	$4.6811*10^{-2}$	$1.8182*10^{-1}$	248	5	$9.7792*10^{-9}$	$1.7953*10^{-1}$	$9.05*10^{-4}$

TABLE 3. Numerical Results for Example 4.1

	Regularized Benamou-Brenier $dt=\frac{1}{21}$, $\beta=10^{-5}$, $\alpha=0.5$, TOL $=10^{-8}$, maxit $=40$				Multiple Shooting $dt=\frac{1}{128}$, $\Delta t=\frac{dt}{32}$, TOL $=10^{-12}$, maxit $=20$				1-d MA: Explicit RK-4		
dx	Map Error	$g_W(\rho_0,\rho_1)$	Time	Newton	Map Error	$g_W(\rho_0,\rho_1)$	Time	Newton	Map Error	$g_W(\rho_0,\rho_1)$	Time
$\frac{1}{16}$	$2.4776*10^{-2}$	$6.3886*10^{-2}$	6.61	26	$3.1463*10^{-2}$	$6.6372*10^{-2}$	2.51	5	$1.7424*10^{2}$	20.261	$3.40*10^{-2}$
$\frac{1}{32}$	$2.1508*10^{-2}$	$6.2688*10^{-2}$	27.6	27	$3.4132*10^{-2}$	$6.5357*10^{-2}$	4.28	5	$6.8561*10^{1}$	5.4739	$2.87*10^{-2}$
$\frac{1}{64}$	$1.5208*10^{-2}$	$6.2503*10^{-2}$	143	27	$3.1703*10^{-2}$	$6.5075*10^{-2}$	16.5	6	$1.5420*10^{-3}$	$6.2603*10^{-2}$	$6.00*10^{-2}$
$\frac{1}{128}$	$1.1248*10^{-2}$	$6.2494*10^{-2}$	939	27	$3.2718*10^{-2}$	$6.5012*10^{-2}$	308	6	$9.5382*10^{-4}$	$6.2678*10^{-2}$	$1.02*10^{-3}$

TABLE 4. Numerical Results for Example 4.2

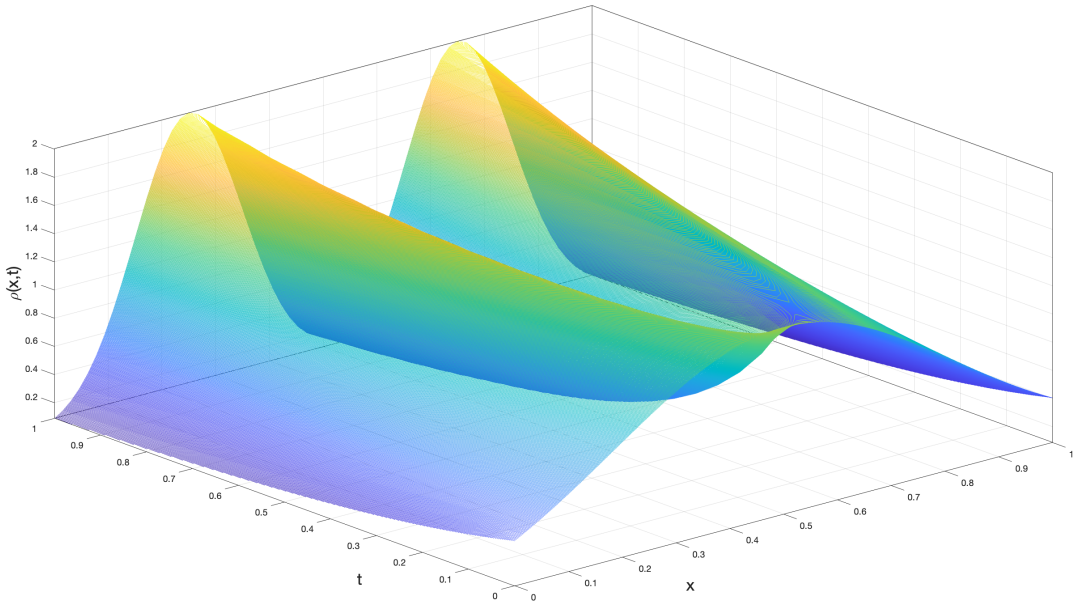

FIGURE 3. Evolution of probability density in Example 4.2 with $dx=\frac{1}{64}$, solved with the regularized Benamou-Brenier method

Example 4.3. *Here we have nonuniform periodic densities*

$$X=Y=[0,1] \mod 1,\ \ \rho_0(x)=1-\frac{1}{32}\cos(2\pi(x+0.5)),\ \ \rho_1(y)=1-\frac{1}{32}\cos(2\pi y)\ .$$

As it can be seen from Table 5, all three methods exhibit expected order of convergence for the map. However, the regularized Benamou-Brenier method show some instability at $x = 1$ for the density evolution, see Figure 4. This is because this method assumes zero flux condition at the boundaries, and this condition is violated for periodic problems. For the discretization of the geodesic equation, we used the scheme in Section 2.2.3, and single shooting proved adequate on this problem.

	Regularized Benamou-Brenier $dt = \frac{1}{21}$, $\beta = 10^{-5}$, $\alpha = 0.5$, $\texttt{TOL} = 10^{-8}$, $\texttt{maxit} = 40$				**Multiple Shooting** $dt = \frac{1}{128}$, $\Delta t = dt$, $\texttt{TOL} = 10^{-5}$, $\texttt{maxit} = 10$				**1-d MA: Shooting Method with RK-4** $\texttt{TOL} = 10^{-12}$		
dx	**Map Error**	$g_W(\rho_0, \rho_1)$	**Time**	**Newton**	**Map Error**	$g_W(\rho_0, \rho_1)$	**Time**	**Newton**	**Map Error**	$g_W(\rho_0, \rho_1)$	**Time**
$\frac{1}{16}$	$1.5127 * 10^{-3}$	$7.7011 * 10^{-3}$	3.96	19	FAIL (Singular Jacobian)				$9.7941 * 10^{-8}$	$7.0329 * 10^{-3}$	1.0595
$\frac{1}{32}$	$8.6542 * 10^{-4}$	$7.3647 * 10^{-3}$	15.6	19	1.4069	1.3346	$1.44 * 10^{-2}$	9	$6.0470 * 10^{-9}$	$7.0329 * 10^{-3}$	1.4939
$\frac{1}{64}$	$4.5942 * 10^{-4}$	$7.1982 * 10^{-3}$	93.5	19	$6.1075 * 10^{-2}$	$5.9121 * 10^{-2}$	$2.40 * 10^{-2}$	4	$3.7646 * 10^{-10}$	$7.0329 * 10^{-3}$	1.9254
$\frac{1}{128}$	$2.3887 * 10^{-4}$	$7.1154 * 10^{-3}$	559	19	$3.4884 * 10^{-3}$	$7.7983 * 10^{-3}$	$8.18 * 10^{-2}$	4	$2.4216 * 10^{-11}$	$7.0329 * 10^{-3}$	1.6242

TABLE 5. Numerical Results for Example 4.3

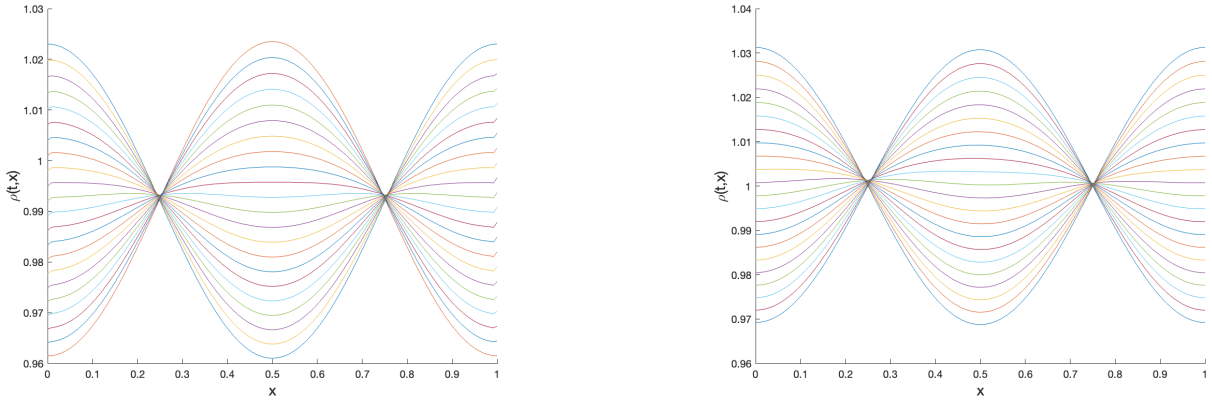

(A) Regularized Benamou-Brenier Method (B) Multiple Shooting Method

FIGURE 4. Evolution of probability density in Example 4.3 with $dx = \frac{1}{128}$

Example 4.4. *This is Example 4.4 of [6]. We have*

$$X = Y = [0, 2], \quad \rho_0(x) = \frac{1}{2}, \quad \rho_1(y) = ce^{-25(y-1)^2} \ ,$$

where c is the normalization constant.

Table 6 shows numerical results for this Example 4.4. Similar to Example 4.2, the explicit RK4 method to solve the Monge-Ampére problem initially gives large error but it eventually shows a fourth order decrease in the error as dx gets smaller. Neither of the Benamou-Brenier methods show convergence. The most likely reasons for this fact are that ρ_1 is nearly 0 near the end-points, and for the method based on the formulation of Section 2.1.3 the truncation from the infinite domain does not hold for a constant density.

	Regularized Benamou-Brenier $dt = \frac{1}{21}$, $\beta = 10^{-5}$, $\alpha = 0.5$, $\texttt{TOL} = 10^{-8}$, $\texttt{maxit} = 40$				**Multiple Shooting** $dt = \frac{1}{60}$, $\Delta t = \frac{dt}{20}$, $\texttt{TOL} = 10^{-12}$, $\texttt{maxit} = 20$				**1-d MA: Explicit RK-4**		
dx	**Map Error**	$g_W(\rho_0, \rho_1)$	**Time**	**Newton**	**Map Error**	$g_W(\rho_0, \rho_1)$	**Time**	**Newton**	**Map Error**	$g_W(\rho_0, \rho_1)$	**Time**
0.1	$4.2075 * 10^{-1}$	$1.6099 * 10^{-1}$	11.3	30	$3.1705 * 10^{-1}$	$5.9022 * 10^{-1}$	3.74	8	$9.8686 * 10^{1}$	$5.6616 * 10^{1}$	$5.8265 * 10^{-2}$
0.05	$4.8934 * 10^{-1}$	$1.5549 * 10^{-1}$	52.7	30	$4.3462 * 10^{-1}$	$5.9402 * 10^{-1}$	2.76	8	$9.7865 * 10^{1}$	$5.5880 * 10^{1}$	$4.5646 * 10^{-2}$
0.025	$5.6196 * 10^{-1}$	$1.5288 * 10^{-1}$	318	31	$5.7931 * 10^{-1}$	$5.9005 * 10^{-1}$	7.84	9	$2.7722 * 10^{-2}$	$4.3975 * 10^{-1}$	$8.4420 * 10^{-2}$
0.0125	$6.1689 * 10^{-1}$	$1.5163 * 10^{-1}$	2052	30	$6.4925 * 10^{-1}$	$5.8709 * 10^{-1}$	33.4	11	$2.4734 * 10^{-2}$	$4.4027 * 10^{-1}$	$1.6293 * 10^{-1}$
0.00625	FAIL (Out of Time)				FAIL (Singular Jacobian)				$1.2359 * 10^{-3}$	$4.4021 * 10^{-1}$	$3.2514 * 10^{-1}$

TABLE 6. Numerical Results for Example 4.4

4.2. **Problems and Results for Separable 2D Examples.** These are all separable 2-d problems. For all of these, we either have the exact optimal map, or can compute using the technique outlined at the beginning of Section 4.1.

Example 4.5. *This is similar to Example 4.1, and here the formulation* (7) *does not hold, since the implied BCs do not hold. We have*

$$X = Y = [0,1] \times [-1,1], \;\; \rho_0(x) = \frac{1}{12}[(2x_1+1)(x_2+3)], \;\; \rho_1(y) = \frac{1}{12}[(3-2y_1)(3-y_2)]$$

and the optimal transport map is

$$T(x_1, x_2) = \begin{pmatrix} \frac{1}{2}(3 - \sqrt{9 - 4x_1 - 4x_1^2}) \\ 3 - \sqrt{11 - 6x_2 - x_2^2} \end{pmatrix}.$$

Table 7 shows numerical results for this example. Since Example 4.5 can be reformulated as two 1D problems, which are similar to Example 4.1, the Regularized Benamou-Brenier and RK4 algorithms give first and fourth orders of convergence for the optimal map, respectively. Surprisingly, we see decrease in error for the multiple shooting method, but not of the nominal order of 1.

	Regularized Benamou-Brenier $dt = \frac{1}{21}$, $\beta = 10^{-5}$, $\alpha = 0.5$, $\texttt{TOL} = 10^{-8}$, $\texttt{maxit} = 40$				**Multiple Shooting** $dt = \frac{1}{128}$, $\Delta t = \frac{dt}{32}$, $\texttt{TOL} = 10^{-12}$, $\texttt{maxit} = 20$				**Two 1-d MA: Explicit RK-4**		
dx	**Map Error**	$g_W(\rho_0, \rho_1)$	**Time**	**Newton**	**Map Error**	$g_W(\rho_0, \rho_1)$	**Time**	**Newton**	**Map Error**	$g_W(\rho_0, \rho_1)$	**Time**
$\frac{1}{16}$	$4.7129 * 10^{-2}$	$5.1595 * 10^{-2}$	8.26	[26, 25]	$7.0847 * 10^{-2}$	$5.3654 * 10^{-2}$	6.58	[5, 5]	$2.4340 * 10^{-5}$	$4.3364 * 10^{-2}$	$5.01 * 10^{-3}$
$\frac{1}{32}$	$2.3748 * 10^{-2}$	$4.7455 * 10^{-2}$	34.8	[26, 25]	$5.7057 * 10^{-2}$	$4.8140 * 10^{-2}$	17.9	[5, 5]	$2.0546 * 10^{-6}$	$4.3368 * 10^{-2}$	$3.81 * 10^{-3}$
$\frac{1}{64}$	$1.1954 * 10^{-2}$	$4.5355 * 10^{-2}$	215	[26, 25]	$5.0202 * 10^{-2}$	$4.5506 * 10^{-2}$	273	[5, 5]	$1.4717 * 10^{-7}$	$4.3368 * 10^{-2}$	$1.49 * 10^{-2}$
$\frac{1}{128}$	$7.3160 * 10^{-3}$	$4.4313 * 10^{-2}$	1350	[26, 25]	FAIL (Out of Memory)				$9.7792 * 10^{-9}$	$4.3368 * 10^{-2}$	$5.88 * 10^{-3}$

TABLE 7. Numerical Results for Example 4.5

Example 4.6. *This is an instance of a mapping of a Gaussian to uniform distribution. This example was also used in [14] and [6], but separability was not exploited in these works. We have*

$$X = Y = [0,1]^2, \;\; \rho_0(x) = \rho_0(x) = c_0 e^{-2[(x_1-0.25)^2 + (x_2-0.75)^2]} \;\; , \;\; \rho_1(y_1, y_2) = 1,$$

where c_0 is the normalization constant so that $\int_X \rho_0 dx = 1$. The optimal transport map is

$$T(x_1,x_2) = \begin{pmatrix} c_1 \int_0^{x_1} e^{-2(s-0.25)^2} ds \\ c_2 \int_0^{x_2} e^{-2(s-0.75)^2} ds \end{pmatrix}, \quad c_1 = \frac{1}{\int_0^1 e^{-2(s-0.25)^2} ds}, \quad c_2 = \frac{1}{\int_0^1 e^{-2(s-0.75)^2} ds}.$$

As it can be seen from Table 8, in Example 4.6 all three numerical methods show decrease in optimal map's error as dx gets smaller. However, once again only Regularized Benamou-Brenier and Runge-Kutta methods show the order. Notice that Regularized Benamou-Brenier algorithm does not have linear decrease in the last row, which can be indicating that one needs to decrease dt and/or β values to get better convergence.

	Regularized Benamou-Brenier $dt=\frac{1}{21}$, $\beta=10^{-5}$, $\alpha=0.5$, TOL $=10^{-8}$, maxit $=40$				**Multiple Shooting** $dt=\frac{1}{128}$, $\Delta t=\frac{dt}{32}$, TOL $=10^{-12}$, maxit $=20$				**Two 1-d MA: Explicit RK-4**		
dx	**Map Error**	$g_W(\rho_0,\rho_1)$	**Time**	**Newton**	**Map Error**	$g_W(\rho_0,\rho_1)$	**Time**	**Newton**	**Map Error**	$g_W(\rho_0,\rho_1)$	**Time**
$\frac{1}{16}$	$1.9393*10^{-2}$	$7.8880*10^{-3}$	9.31	[25, 25]	$3.7402*10^{-2}$	$8.3962*10^{-3}$	4.68	[5, 5]	$8.0319*10^{-8}$	$6.6608*10^{-3}$	$2.75*10^{-2}$
$\frac{1}{32}$	$9.5747*10^{-3}$	$7.2625*10^{-3}$	41.1	[25, 25]	$2.6983*10^{-2}$	$7.3999*10^{-3}$	8.82	[5, 5]	$5.0100*10^{-9}$	$6.6607*10^{-3}$	$2.48*10^{-2}$
$\frac{1}{64}$	$4.8743*10^{-3}$	$6.9575*10^{-3}$	237	[25, 25]	$2.2044*10^{-2}$	$6.9299*10^{-3}$	27.3	[5, 5]	$3.1351*10^{-10}$	$6.6607*10^{-3}$	$4.23*10^{-2}$
$\frac{1}{128}$	$3.1003*10^{-3}$	$6.8079*10^{-3}$	1501	[25, 25]	$1.9558*10^{-2}$	$6.7029*10^{-3}$	517	[5, 5]	$1.9593*10^{-11}$	$6.6607*10^{-3}$	$6.87*10^{-2}$

TABLE 8. Numerical Results for Example 4.6

Example 4.7. *We have*

$$X = Y = \mathbb{T}^2, \;\; \rho_0(x_1,x_2) = (1 - \frac{1}{32}\sin(2\pi x_1))(1 - \frac{1}{32}\cos(2\pi x_2)), \;\; \rho_1(y_1,y_2) = 1,$$

where $\mathbb{T}^2 = [0,1]^2$ is the 2-torus. The optimal transport map is:

$$T(x_1,x_2) = \begin{pmatrix} x_1 + \frac{1}{64\pi}\cos(2\pi x_1) \\ x_2 - \frac{1}{64\pi}\sin(2\pi x_2) \end{pmatrix}.$$

Table 9 shows numerical results for this example. For this periodic, and separable, problem, the discretization of Section 2.2.3 outperformed the Regularized Benamou-Brenier method, and single shooting to find the initial velocity was adequate. Nevertheless, the explicit RK4 method still gives the best result among all three methods.

	Regularized Benamou-Brenier $dt=\frac{1}{21}$, $\beta=10^{-5}$, $\alpha=0.5$, TOL $=10^{-8}$, maxit $=40$				**Multiple Shooting** $dt=\frac{1}{128}$, $\Delta t=dt$, TOL $=10^{-5}$, maxit $=50$				**Two 1-d MA: Explicit RK-4**		
dx	**Map Error**	$g_W(\rho_0,\rho_1)$	**Time**	**Newton**	**Map Error**	$g_W(\rho_0,\rho_1)$	**Time**	**Newton**	**Map Error**	$g_W(\rho_0,\rho_1)$	**Time**
$\frac{1}{16}$	$9.7683*10^{-4}$	$1.1674*10^{-5}$	8.03	[22, 17]	FAIL (Singular Jacobian)				$8.2517*10^{-8}$	$1.2368*10^{-5}$	$1.89*10^{-2}$
$\frac{1}{32}$	$4.3948*10^{-4}$	$1.2001*10^{-5}$	34.9	[24, 17]	FAIL (Singular Jacobian)				$5.1396*10^{-9}$	$1.2368*10^{-5}$	$3.86*10^{-3}$
$\frac{1}{64}$	$2.3508*10^{-4}$	$1.2181*10^{-5}$	207	[26, 17]	$4.5351*10^{-6}$	$1.2184*10^{-5}$	0.13	[10, 10]	$3.2095*10^{-10}$	$1.2368*10^{-5}$	$3.24*10^{-3}$
$\frac{1}{128}$	$1.2172*10^{-4}$	$1.2270*10^{-5}$	1342	[28, 17]	$1.1279*10^{-6}$	$1.2274*10^{-5}$	0.17	[4, 4]	$2.0054*10^{-11}$	$1.2368*10^{-5}$	$2.69*10^{-3}$
$\frac{1}{256}$	FAIL (Out of Time)				$7.1512*10^{-7}$	$1.2320*10^{-5}$	0.45	[3, 3]	$1.2537*10^{-12}$	$1.2368*10^{-5}$	$5.05*10^{-3}$

TABLE 9. Numerical Results for Example 4.7

Example 4.8. *This is a problem used in [1] and in [23]. We have*

$$X = Y = [0,1]^2, \quad \rho_0(x) = ce^{-10[(x_1-0.5)^2+(x_2-0.5)^2]}, \ \ \rho_1(y) = \rho_0(y_1 + 0.5 \ [\text{mod } 1], y_2 + 0.5 \ [\text{mod } 1])$$

where c is the normalization constant.

As Table 10 shows, only the explicit RK4 method shows convergence with desired order. Both Benamou-Brenier algorithms converge with small error but order is not there and give different values for the Wasserstein distance. Figure 5 shows density evolution for this example, which was constructed through hybrid technique and matches that reported in [1].

	Regularized Benamou-Brenier $dt = \frac{1}{21}$, $\beta = 10^{-5}$, $\alpha = 0.5$, $\texttt{TOL} = 10^{-8}$, $\texttt{maxit} = 40$				**Multiple Shooting** $dt = \frac{1}{128}$, $\Delta t = \frac{dt}{32}$, $\texttt{TOL} = 10^{-12}$, $\texttt{maxit} = 20$				**Two 1-d MA: Explicit RK-4**		
dx	**Map Error**	$g_W(\rho_0,\rho_1)$	**Time**	**Newton**	**Map Error**	$g_W(\rho_0,\rho_1)$	**Time**	**Newton**	**Map Error**	$g_W(\rho_0,\rho_1)$	**Time**
$\frac{1}{16}$	$4.2148 * 10^{-2}$	$3.5447 * 10^{-2}$	11.5	[28, 18]	$1.0370 * 10^{-1}$	$3.3534 * 10^{-2}$	8.12	[6, 6]	$9.2316 * 10^{-2}$	$2.8575 * 10^{-2}$	$5.48 * 10^{-2}$
$\frac{1}{32}$	$2.9934 * 10^{-2}$	$3.1972 * 10^{-2}$	59.1	[27, 27]	$8.6082 * 10^{-2}$	$3.0213 * 10^{-2}$	10.7	[6, 6]	$1.7530 * 10^{-2}$	$2.9157 * 10^{-2}$	$5.88 * 10^{-2}$
$\frac{1}{64}$	$2.1585 * 10^{-2}$	$3.0434 * 10^{-2}$	327	[28, 28]	$7.7826 * 10^{-2}$	$2.8763 * 10^{-2}$	35.8	[7, 7]	$1.9884 * 10^{-3}$	$2.9259 * 10^{-2}$	$1.11 * 10^{-1}$
$\frac{1}{128}$	$2.1062 * 10^{-2}$	$2.9719 * 10^{-2}$	2154	[28, 28]	$7.4088 * 10^{-2}$	$2.8092 * 10^{-2}$	607	[7, 7]	$1.5436 * 10^{-4}$	$2.9272 * 10^{-2}$	$2.15 * 10^{-1}$

TABLE 10. Numerical Results for Example 4.8

4.3. **Problems and Results for Non-Separable 2D Examples.** Last, we consider two non-separable 2-d problems.

Example 4.9. *We have*

$$X = Y = [-0.5, 0.5]^2, \quad \rho_1(y) = 1$$

and

$$\begin{aligned}\rho_0(x) = &\Big(a_1 + a_2 e^{0.5x_1^2} x_1 + 0.01\pi \sin(\pi x_1)\sin(\pi x_2)\Big) \\ &\Big(b_1 + b_2 e^{0.5x_2^2} x_2 + 0.01\pi \sin(\pi x_1)\sin(\pi x_2)\Big) - 0.01^2\pi^2 \cos^2(\pi x_1)\cos^2(\pi x_2) \\ &a_0 = -1; \quad a_1 = 1; \quad a_2 = -a_0 e^{-0.125}; b_0 = -1; \quad b_1 = 1; \quad b_2 = -b_0 e^{-0.125}.\end{aligned}$$

The optimal transport map is:

$$T(x_1, x_2) = \begin{pmatrix} a_0 + a_1 x_1 + a_2 e^{0.5x_1^2} - 0.01\cos(\pi x_1)\sin(\pi x_2) \\ b_0 + b_1 x_2 + b_2 e^{0.5x_2^2} - 0.01\sin(\pi x_1)\cos(\pi x_2) \end{pmatrix}$$

Table 11 shows numerical results for Example 4.9. The Monge-Ampere discretization of Section 2.2.1 shows linear convergence to the exact map, as expected. Multiple shooting method has decrease in error too but order is not linear. Regularized Benamou-Brenier method converges, but the error is large and not decreasing as dx is halved. In addition, increase in computation time is significant compared to the 1D problems. As a result, evaluations for smaller dx values did not succeed. Figure 6 illustrates density evolution for this example with $dx = \frac{1}{32}$, when solved with multiple shooting method.

Example 4.10. *Here we consider mapping a Gaussian to a two-bumps Gaussian. We have*

$$X = Y = [0,1]^2, \quad \rho_0(x_1, x_2) = c_0 e^{-5[(x_1-0.5)^2+(x_2-0.5)^2]}$$

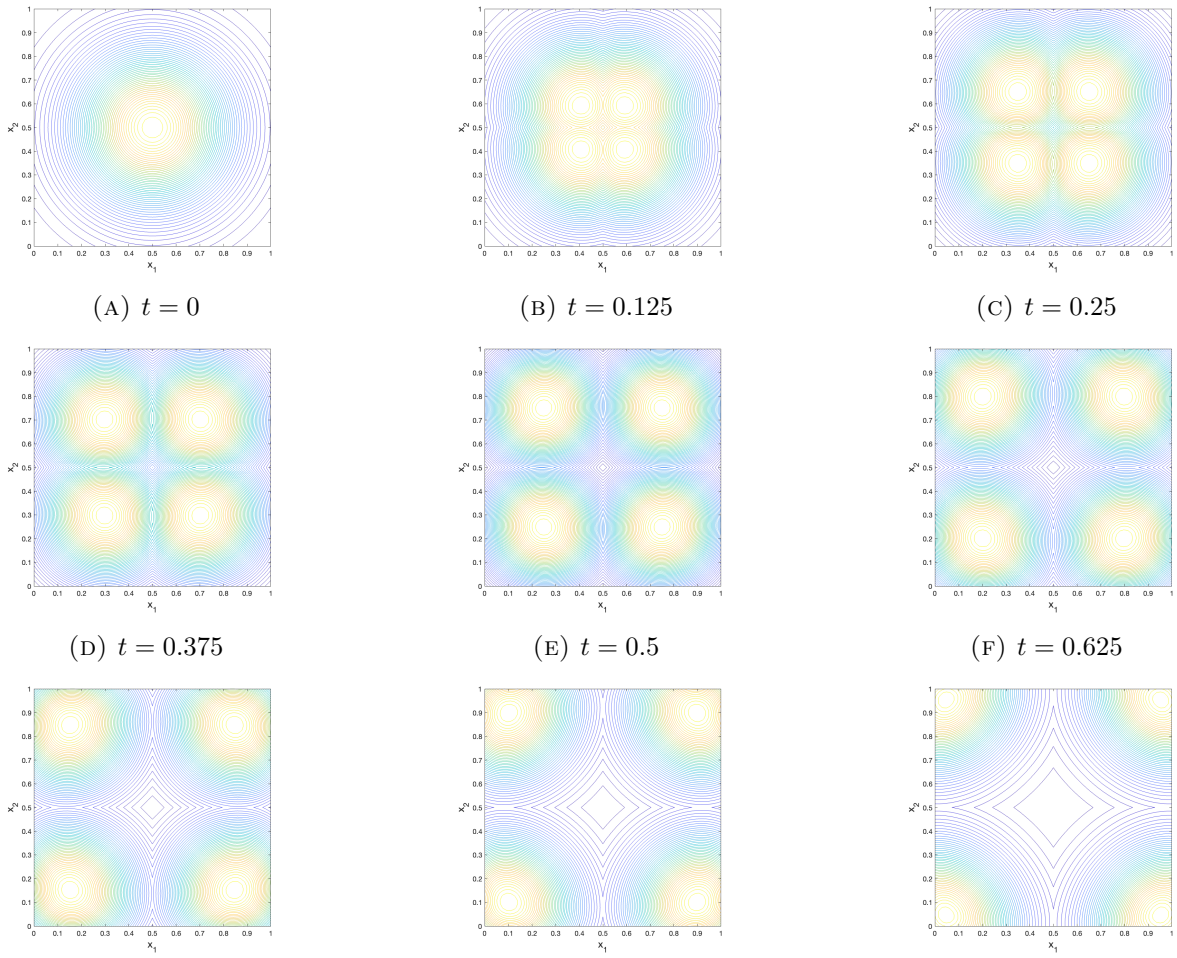

(A) $t = 0$ (B) $t = 0.125$ (C) $t = 0.25$

(D) $t = 0.375$ (E) $t = 0.5$ (F) $t = 0.625$

(G) $t = 0.75$ (H) $t = 0.875$ (I) $t = 1$

FIGURE 5. Evolution of probability density for Example 4.8, solved with the multiple shooting method, $dx = \frac{1}{64}$. Here, we first obtained the initial velocity $v(0, x)$ solving by multiple shooting two 1-d problems, and then integrated in time for ρ and v the system (7) using the time integrator from [6].

	Regularized Benamou-Brenier $dt = \frac{1}{21}$, $\beta = 10^{-3}$, $\alpha = 0.3$, TOL $= 10^{-6}$, maxit $= 40$				**Multiple Shooting** $dt = \frac{1}{21}$, $\Delta t = \frac{dt}{32}$, TOL $= 10^{-5}$, maxit $= 20$				**2-d Monge-Ampere (Identity)** TOL $= 10^{-8}$, maxit $= 20$			
dx	**Map Error**	$g_W(\rho_0, \rho_1)$	**Time**	**Newton**	**Map Error**	$g_W(\rho_0, \rho_1)$	**Time**	**Newton**	**Map Error**	$g_W(\rho_0, \rho_1)$	**Time**	**Newton**
$\frac{1}{8}$	0.12680	$2.4279 * 10^{-3}$	268	11	$5.4786 * 10^{-2}$	$1.5900 * 10^{-1}$	1.74	4	$5.1241 * 10^{-2}$	$1.5014 * 10^{-1}$	0.01	6
$\frac{1}{16}$	0.12823	$1.2956 * 10^{-3}$	4526	4	$3.4618 * 10^{-2}$	$1.3876 * 10^{-1}$	18.9	4	$2.3174 * 10^{-2}$	$1.3623 * 10^{-1}$	0.02	6
$\frac{1}{32}$	FAIL (Out of Time)				$2.4568 * 10^{-2}$	$1.2859 * 10^{-1}$	631	4	$1.1108 * 10^{-2}$	$1.3017 * 10^{-1}$	0.19	8
$\frac{1}{64}$	FAIL (Out of Time)				FAIL (Out of Memory)				$5.4616 * 10^{-3}$	$1.2731 * 10^{-1}$	2.78	9
$\frac{1}{128}$	FAIL (Out of Time)				FAIL (Out of Memory)				$2.7276 * 10^{-3}$	$1.2593 * 10^{-1}$	78.3	17

TABLE 11. Numerical Results for Example 4.9

and

$$\rho_1(y_1, y_2) = c_1[e^{-20[(y_1-0.25)^2+(y_2-0.75)^2]} + e^{-20[(y_1-0.75)^2+(y_2-0.25)^2]}]$$

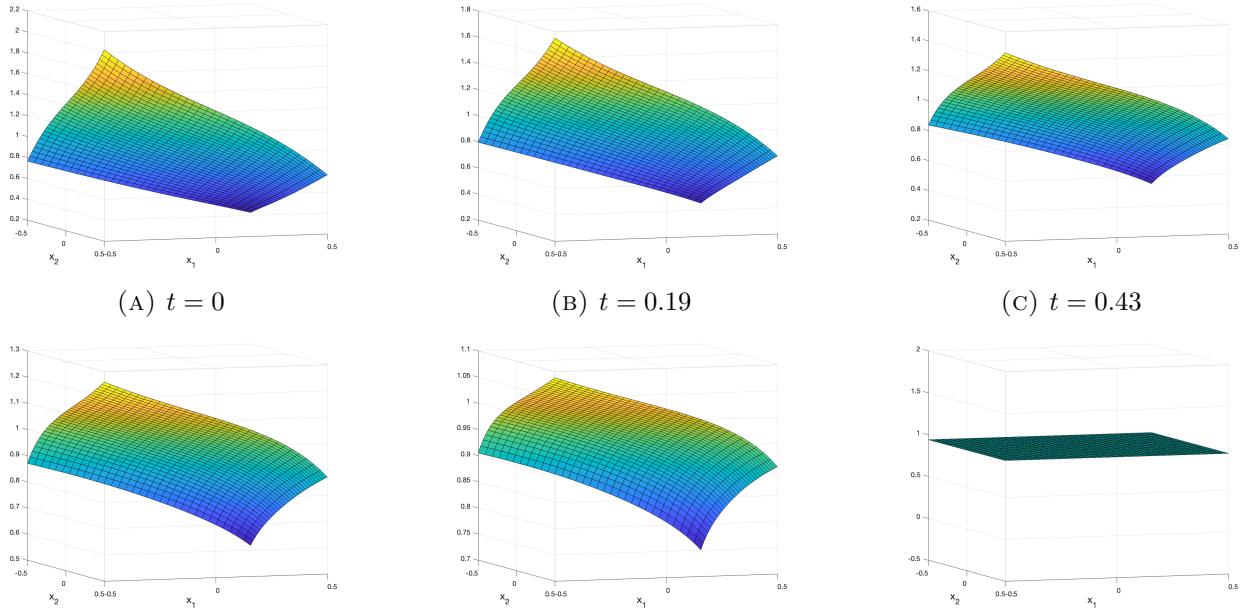

(A) $t = 0$ (B) $t = 0.19$ (C) $t = 0.43$

(D) $t = 0.62$ (E) $t = 0.81$ (F) $t = 1$

FIGURE 6. Evolution of probability density in Example 4.9 with $dx = \frac{1}{32}$, solved with multiple shooting method.

where c_0, c_1 are normalization constants. Here, we do not have an expression for the optimal map.

Table 12 gives the results for this 2D example, showing that the Regularized BB method is very costly to say the least. Figure 7 shows density evolution for this example when solved by multiple shooting method.

	Regularized Benamou-Brenier $dt = \frac{1}{21}$, $\beta = 10^{-3}$, $\alpha = 0.3$, TOL $= 10^{-6}$, maxit $= 40$			**Multiple Shooting** $dt = \frac{1}{21}$, $\Delta t = \frac{dt}{32}$, TOL $= 10^{-5}$, maxit $= 20$			**2-d MA (Identity)** TOL $= 10^{-8}$, maxit $= 20$		
dx	$g_W(\rho_0, \rho_1)$	**Time**	**Newton**	$g_W(\rho_0, \rho_1)$	**Time**	**Newton**	$g_W(\rho_0, \rho_1)$	**Time**	**Newton**
$\frac{1}{8}$	$2.4279 * 10^{-2}$	420	16	$1.8587 * 10^{-1}$	1.96	5	$8.5576 * 10^{-2}$	0.23	7
$\frac{1}{16}$	$3.6912 * 10^{-2}$	10956	9	$1.8737 * 10^{-1}$	24.6	6	$7.9610 * 10^{-2}$	0.50	6
$\frac{1}{32}$	FAIL (Out of Time)			$1.8717 * 10^{-1}$	928	7	$7.6449 * 10^{-2}$	1.91	6
$\frac{1}{64}$	FAIL (Out of Time)			FAIL (Out of Memory)			$7.4841 * 10^{-2}$	9.17	8
$\frac{1}{128}$	FAIL (Out of Time)			FAIL (Out of Memory)			$7.4034 * 10^{-2}$	81.9	12

TABLE 12. Numerical Results for Example 4.10

5. CONCLUSION

In this work, we provided a numerical study of three different methods to solve the classic OT problem with quadratic cost, posed in 1-d or 2-d, restricting to problems posed on finite rectangular domains (intervals in 1-d) or with periodic data, hence posed on the torus. We gave implementation details and numerical comparison of three approaches. The first rests on solving the Monge-Ampére PDE to target the optimal map directly; for periodic problems, our approach is standard (as it was

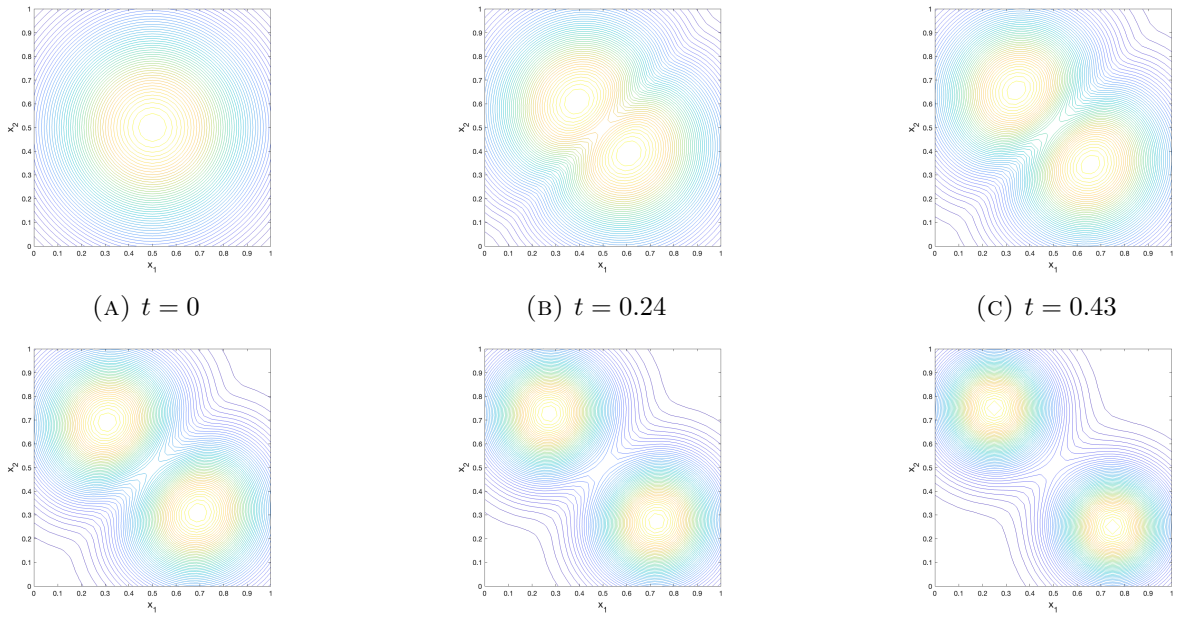

(A) $t = 0$ (B) $t = 0.24$ (C) $t = 0.43$

(D) $t = 0.62$ (E) $t = 0.86$ (F) $t = 1$

FIGURE 7. Evolution of probability density in Example 4.10 with $dx = \frac{1}{32}$, solved with multiple shooting method.

used already in [16]), whereas for problems posed on a rectangular domain we imposed the so-called transport boundary conditions and followed more closely the approach of Froese in [10]. The other two methods are different interpretations/implementations of the fluid–dynamics (Benamou-Brenier) formulation of the problem, and target the entire time evolution of the density, $\rho(t, x)$, from initial to final configurations. In one case, we considered an implementation which is well suited to deal with finite domains, and we followed the regularized minimization approach of [14]. In the other case, we followed the recent interpretation of [6] of the fluid-flow formulation as a pair of PDEs; these PDEs are given on all of $\mathbb{R}^d$ and their use for problems given on the torus is particularly advantageous, whereas their use for truncated domains requires no mass escape from the boundary, which places a potentially unwanted restriction on the problems one can handle. Further, a novel theoretical contribution of our work has been the introduction of separable structure, which is shared by many OT problems. Exploiting this viewpoint proved very valuable in obtaining much more efficient and accurate techniques. Finally, we proposed a hybrid technique, whereby the "exact" initial velocity (found by either solving the Monge-Ampére PDE via the optimal map, or by exploiting separability and using 1-d fluid-flow problems) is fed into the time stepping scheme of [6] in order to recover the time evolution of the density.

With similar level of sophistication in implementing the various techniques, our results show that if one is interested in the optimal map (the Monge map), then direct solution of the Monge-Ampére equation is the most efficient way to proceed, especially when we have, and exploit, separable structure. For those situation where the time evolution of the density is needed (as it is the case when we want to find the geoedesic trajectory), then the two formulations of [14] and [6] offer some advantages with respect to each other: (i) in general, the formulation of [6] is less costly than that of [14], and

outperforms it for periodic problems, but (ii) on a truncated domain the formulation of [14] performs better, though it remains somewhat expensive. In the end, although one can find justification for failure of any of the techniques we considered, in our opinion this defeats the purpose of a well designed numerical method for solving the OT problem: one should assume that it delivers the desired result and not wander why it does not. In this light, the hybrid technique of Section 2.3 proved to be a simple and effective way to obtain the density evolution for separable problems, without having to solve large nonlinear systems, and we recommend adopting it whenever applicable and the density evolution is desired.

References

[1] Jean-David Benamou and Yann Brenier. A computational fluid mechanics solution to the monge-kantorovich mass transfer problem. *Numerische Mathematik*, 84(3):375–393, 2000.

[2] Jean-David Benamou, Brittany D Froese, and Adam M Oberman. Numerical solution of the optimal transportation problem using the monge–ampère equation. *Journal of Computational Physics*, 260:107–126, 2014.

[3] Rainer Burkard, Mauro Dell'Amico, and Silvano Martello. *Assignment Problems*. Society for Industrial and Applied Mathematics, 2012.

[4] Luis A. Caffarelli, Sergey A. Kochengin, and Vladimir I. Oliker. On the numerical solution of the problem of reflector design with given far-field scattering data. In *Monge Ampère equation: applications to geometry and optimization (NSF-CBMS Conference on the Monge Ampère Equation, Applications to Geometry and Optimization, July 9–13, 1997, Florida Atlantic University)*, volume 226 of *Contemporary Mathematics*, pages 13–32, Providence, R.I., 1999. American Mathematical Society.

[5] Rick Chartrand, Brendt Wohlberg, Kevin Vixie, and Erik Bollt. A gradient descent solution to the Monge-Kantorovich problem. *Applied Mathematical Sciences*, 3:1071–1080, 2009.

[6] Jianbo Cui, Luca Dieci, and Haomin Zhou. A continuation multiple shooting method for wasserstein geodesic equation. *SIAM Journal on Scientific Computing*, 44(5):A2918–A2943, 2022.

[7] Marco Cuturi. Sinkhorn distances: Lightspeed computation of optimal transport. *Advances in neural information processing systems*, 26, 2013.

[8] Luca Dieci and Joseph D. Walsh III. The boundary method for semi-discrete optimal transport partitions and wasserstein distance computation. *Journal of Computational and Applied Mathematics*, 353:318–344, 2019.

[9] Brittany D Froese. A numerical method for the elliptic monge–ampère equation with transport boundary conditions. *SIAM Journal on Scientific Computing*, 34(3):A1432–A1459, 2012.

[10] Brittany D. Froese and Adam M. Oberman. Convergent finite difference solvers for viscosity solutions of the elliptic Monge-Ampère equation in dimensions two and higher. *Journal of Computational Physics*, 260:107–126, 2014.

[11] Leonid V. Kantorovich. On the transfer of masses. In *Dokl. Akad. Nauk. SSSR*, 1942.

[12] Christian Léonard. A survey of the schr\" odinger problem and some of its connections with optimal transport. *Discrete and continuous dynamical systems*, 34(4):1533–1574, 2014.

[13] Bruno Lévy. A numerical algorithm for l2 semi-discrete optimal transport in 3d. *ESAIM: Mathematical Modelling and Numerical Analysis*, 49(6):1693–1715, 2015.

[14] Wuchen Li, Penghang Yin, and Stanley Osher. Computations of optimal transport distance with Fisher information regularization. *Journal of Scientific Computing*, 75(3):1581–1595, 2018.

[15] Wuchen Li and Jiaxi Zhao. Wassserstein information matrix. *Information Geometry*, 2023.

[16] Grégoire Loeper and Francesca Rapetti. Numerical solution of the monge–ampère equation by a newton's algorithm. *Comptes Rendus Mathematique*, 340(4):319–324, 2005.

[17] Quentin Mérigot. A multiscale approach to optimal transport. In *Computer Graphics Forum*, volume 30, pages 1583–1592. Wiley Online Library, 2011.

[18] Ludovic Métivier, Romain Brossier, Quentin Mérigot, Edouard Oudet, and Jean Virieux. Measuring the misfit between seismograms using an optimal transport distance: Application to full waveform inversion. *Geophysical Supplements to the Monthly Notices of the Royal Astronomical Society*, 205(1):345–377, 2016.

[19] Jean-Marie Mirebeau. Discretization of the 3D Monge-Ampère operator, between wide stencils and power diagrams. arXiv:1503.00947, 2015.

[20] Gaspard Monge. Mémoire sur la théorie des déblais et des remblais. *Mem. Math. Phys. Acad. Royale Sci.*, pages 666–704, 1781.

[21] Gyutaek Oh, Byeongsu Sim, HyungJin Chung, Leonard Sunwoo, and Jong Chul Ye. Unpaired deep learning for accelerated mri using optimal transport driven cyclegan. *IEEE Transactions on Computational Imaging*, 6:1285–1296, 2020.

[22] Vladimir I. Oliker and Laird D. Prussner. On the numerical solution of the equation $\frac{\partial^2 z}{\partial x^2}\frac{\partial^2 z}{\partial y^2} - \left(\frac{\partial^2 z}{\partial x \partial y}\right)^2 = f$ and its discretizations, *I. Numerische Mathematik*, 54:271–293, 1988.

[23] Filippo Santambrogio. Optimal transport for applied mathematicians. *Birkäuser, NY*, 55(58-63):94, 2015.

[24] Mohamed M. Sulman, JF Williams, and Robert D. Russell. An efficient approach for the numerical solution of the monge–ampère equation. *Applied Numerical Mathematics*, 61(3):298–307, 2011.

[25] Cedric Villani. *Optimal transport*, volume 338 of *Grundlehren der Mathematischen Wissenschaften [Fundamental Principles of Mathematical Sciences]*. Springer-Verlag, Berlin, 2009. Old and new.

Appendix

Consider the two-point boundary value problem (cfr. with (22))

$$\begin{cases} \rho_1(y)y' = \rho_0(x) \\ y(a) = \alpha, \quad y(b) = \beta \end{cases} \tag{32}$$

where

$$\int_a^b \rho_0(x)dx = \int_\alpha^\beta \rho_1(y)dy = 1$$
$$\rho_0(x) > 0, \quad \forall x \in [a,b], \quad \rho_1(y) > 0, \quad \forall y \in [\alpha,\beta].$$

Claim. *The boundary value problem (32) is well-posed in the sense of Hadamard.*

Proof. The existence and uniqueness of the solution is a consequence of results for the Monge-Ampére equation. We observe that the solution y of (32) can be expressed implicity using the cumulative distribution functions $R_0(x) = \int_a^x \rho_0(s)ds$ and $R_1(y) = \int_\alpha^y \rho_1(z)dz$, that is from the relation

$$R_1(y) = R_0(x) \tag{33}$$

where $R_0(a) = 0$, $R_0(b) = 1$, $R_1(\alpha) = 0$, and $R_1(\beta) = 1$.

We show the continuous dependence on the data, therefore consider four possible perturbations, in α, in β, in ρ_0, and in ρ_1.

• Perturbation in α. Consider

$$\begin{aligned} &\rho_1(\tilde{y})\tilde{y}' = \rho_0(x) \\ &\tilde{y}(a) = \alpha + \varepsilon, \quad \tilde{y}(b) = \tilde{\beta} \end{aligned} \tag{34}$$

where $|\varepsilon|$ is small, and $\int_{\alpha+\varepsilon}^{\tilde{\beta}} \rho_1(z)dz = 1$ holds. Then, the solution of (34) satisfies:

$$\int_{\alpha+\varepsilon}^{\tilde{y}} \rho_1(z)dz = \int_a^x \rho_0(s)ds \tag{35}$$

From (33): $\int_\alpha^y \rho_1(z)dz = \int_a^x \rho_0(s)ds$. As a result, it follows that:

$$0 = \int_{\alpha+\varepsilon}^{\tilde{y}} \rho_1(z)dz - \int_\alpha^y \rho_1(z)dz = \int_\alpha^{\tilde{y}} \rho_1(z)dz - \int_\alpha^{\alpha+\varepsilon} \rho_1(z)dz - \int_\alpha^y \rho_1(z)dz,$$
$$0 = \int_y^{\tilde{y}} \rho_1(z)dz - \int_\alpha^{\alpha+\varepsilon} \rho_1(z)dz \implies \int_y^{\tilde{y}} \rho_1(z)dz = \int_\alpha^{\alpha+\varepsilon} \rho_1(z)dz$$
$$\left| \int_y^{\tilde{y}} \rho_1(z)dz \right| \leq \int_{\min(y,\tilde{y})}^{\max(y,\tilde{y})} \rho_1(z)dz \leq |\varepsilon| \max_z |\rho_1(z)| \implies |y-\tilde{y}| \leq |\varepsilon| \frac{\max_z |\rho_1(z)|}{\min_z |\rho_1(z)|}$$

• Perturbation in β. This proceeds similarly to the above. Considering

$$\begin{aligned} &\rho_1(\tilde{y})\tilde{y}' = \rho_0(x) \\ &\tilde{y}(a) = \tilde{\alpha}, \quad \tilde{y}(b) = \beta + \varepsilon, \end{aligned} \tag{36}$$

where $|\varepsilon|$ is small and $\int_{\tilde{\alpha}}^{\beta+\varepsilon} \rho_1(z)dz = 1$ holds, one now obtains

$$|y-\tilde{y}| \leq |\varepsilon| \frac{\max_z |\rho_1(z)|}{\min_z |\rho_1(z)|} \ .$$

• Perturbation of $\rho_0(x)$. Now we need to consider small zero average perturbations of ρ_0. That is, we consider

$$\begin{aligned} &\rho_1(\tilde{y})\tilde{y}' = \rho_0(x) + \varepsilon(x) \\ &\tilde{y}(a) = \alpha, \quad \tilde{y}(b) = \beta \end{aligned} \tag{37}$$

where $\int_a^b \varepsilon(s)ds = 0$ and $|\varepsilon(x)|$ is small for all x. The solution of (37) satisfies:

$$\int_\alpha^{\tilde{y}} \rho_1(z)dz = \int_a^x \rho_0(s)ds + \int_a^x \varepsilon(s)ds \tag{38}$$

From (33): $\int_\alpha^y \rho_1(z)dz = \int_a^x \rho_0(s)ds$. As a result, it follows that

$$\int_\alpha^{\tilde{y}} \rho_1(z)dz - \int_\alpha^y \rho_1(z)dz = \int_a^x \varepsilon(s)ds \implies \int_y^{\tilde{y}} \rho_1(z)dz = \int_a^x \varepsilon(s)ds$$
$$\left| \int_y^{\tilde{y}} \rho_1(z)dz \right| = \rho_1(\hat{z})|y(x)-\tilde{y}(x)| \implies |y(x)-\tilde{y}(x)| \leq |x-a| \frac{\max_s |\varepsilon(s)|}{\rho_1(\hat{z})}$$

where $\min(y,\tilde{y}) \leq \hat{z} \leq \max(y,\tilde{y})$.

• Perturbation of $\rho_1(\tilde{y})$. This is similar to the previous case. We consider small zero average perturbations of ρ_1:

$$\begin{aligned} &[\rho_1(\tilde{y}) + \varepsilon(\tilde{y})]\tilde{y}' = \rho_0(x) \\ &\tilde{y}(a) = \alpha, \quad \tilde{y}(b) = \beta \end{aligned} \tag{39}$$

where $\int_\alpha^\beta \varepsilon(s)ds = 0$ and $|\varepsilon(\tilde{y})|$ is small for all $\tilde{y}$. The solution of (39) satisfies:

$$\int_\alpha^{\tilde{y}} \rho_1(z)dz + \int_\alpha^{\tilde{y}} \varepsilon(z)dz = \int_a^x \rho_0(s)ds \tag{40}$$

From (33): $\int_\alpha^y \rho_1(z)dz = \int_a^x \rho_0(s)ds$. As a result, it follows that

$$\int_\alpha^y \rho_1(z)dz - \int_\alpha^{\tilde{y}} \rho_1(z)dz = \int_\alpha^{\tilde{y}} \varepsilon(z)dz \implies \int_{\tilde{y}}^y \rho_1(z)dz = \int_\alpha^{\tilde{y}} \varepsilon(z)dz$$

$$\left| \int_y^{\tilde{y}} \rho_1(z)dz \right| = \rho_1(\hat{z})|y(x) - \tilde{y}(x)| \implies |y(x) - \tilde{y}(x)| \leq |\beta - \alpha| \frac{\max_s |\varepsilon(s)|}{\rho_1(\hat{z})}$$

where $\min(y, \tilde{y}) \leq \hat{z} \leq \max(y, \tilde{y})$. □

School of Mathematics, Georgia Institute of Technology, Atlanta, GA 30332 U.S.A.
Email address: dieci@math.gatech.edu

School of Mathematics, Georgia Institute of Technology, Atlanta, GA 30332 U.S.A.
Email address: domarov3@gatech.edu